Investigation of Wind-Induced Highway Lighting Pole Vibration Using Full-Scale Measurement

By Delong Zuo and Christopher Letchford

Notice

The United States Government and the State of Texas do not endorse products or manufacturers. Trade or manufacturers' names appear herein solely because they are considered essential to the object of this report.

Technical Report Documentation Page

1. Report No.: FHWA/TX -08-0-4586-5	2. Government Accession No.:	3. Recipient's Catalog No.:

4. Title and Subtitle:
   Investigation of Wind-Induced Highway Lighting Pole Vibration Using Full-Scale Measurement
		5. Report Date:
		   June 2008

		6. Performing Organization Code:

7. Author(s):
   Delong Zuo and Christopher Letchford
		8. Performing Organization
		   Report No. 0-4586-5

9. Performing Organization Name and Address:
   Texas Tech University
   College of Engineering
   Box 41023
   Lubbock, Texas 79409-1023
		10. Work Unit No. (TRAIS):

		11. Contract or Grant No. : Project 0-4586

12. Sponsoring Agency Name and Address
   Texas Department of Transportation
   Research and Technology
   P. O. Box 5080
   Austin, TX 78763-5080
		13. Type of Report and Period
		   Cover: Technical Report
		September 2004 – August 2007

		14. Sponsoring Agency Code:

15. Supplementary Notes: Project performed in cooperation with the Texas Department of Transportation and the Federal Highway Administration. Revision of AASHTO Fatigue Design Loadings for Signs, Luminaires, and Traffic Signal Structures for Use in Texas

16. Abstract:
Under the excitation from wind, some highway lighting poles have exhibited large-amplitude vibrations. Such unexpected vibrations have resulted in premature failure of, or damage to, these structures. To investigate the mechanism of these wind-induced vibrations, a long-term full-scale measurement project was conducted at Texas Tech University under the sponsorship of Texas Department of Transportation. Interpretation of the recorded lighting pole vibrations and the corresponding wind revealed two types of wind excitation mechanism: buffeting, which is responsible for large-amplitude vibrations in the first in-plane and out-of-plane modes of the structure, and vortex-shedding, under specific wind conditions, which induces vibrations of the structure in the higher modes. This report describes the full-scale monitoring campaign and summarizes the results obtained from this effort.

17. Key Words Lighting pole, vortex shedding, buffeting, wind, fatigue	18. Distribution Statement: No restrictions. This document is available to the public through the National Technical Information Service, Springfield, VA 22161, www.ntis.gov		

19. Security Classif. (of this report)
   Unclassified
	20. Security Classif. (of this page)
	   Unclassified
		21. No. of Pages
		42
			22. Price

Form DOT F 1700.7 (8-72)

Investigation of Wind-Induced Highway Lighting Pole Vibration Using Full-Scale Measurement

by

Delong Zuo, Ph.D and Christopher Letchford, Ph.D

Department of Civil and Environmental Engineering

Texas Tech University

Disclaimer

The contents of this report reflect the views of the authors who are responsible for the facts and accuracy of the data presented herein. The contents do not necessarily reflect the official view or policies of the Texas Department of Transportation. This report does not constitute a standard, specification or regulation.

Acknowledgement

Table of Contents

List of Figures

List of Tables

1   Introduction

Highway lighting poles as slender flexible structures with low-level of inherent damping have been observed to exhibit wind-induced vibrations. If not mitigated, such vibration can result in fatigue of some structural members (e.g., Peil and Behrens 2002) and, in some extreme cases, the collapse of these structures (Caracoglia and Jones 2007).

Current design of highway lighting poles are based on the fourth edition of the "AASHTO Standard Specifications for Structural Supports for Highway Signs, Luminaires and Traffic Signals" (AASHTO 2001), which provides standardized design procedures and examples. Limitations, however, still exist in these specifications. The wind loading specified by these procedures are primarily based on results from previous wind tunnel (Kaczinski et al. 1998) and water tank tests (McDonald et al. 1995) but not a thorough understanding of the prototype wind-excitation mechanism. Also, in the specifications, attention is devoted to the design of "high-level lighting poles", which are normally 55ft or more in height, and the "typical lighting poles" often found along highways, which are usually 30 ft to 55 ft in height, are often overlooked. For example, in the "Fatigue Design" section of the specifications, the shorter lighting poles are not recommended to be designed for fatigue since they are considered "smaller structures". Recently, much effort has been made to understand the aerodynamic behavior of lighting pole structures and the corresponding fatigue characteristics using field measurements (e.g.,Connor et al. 2007; Dexter 2004; Foley et al. 2004; Van de Lindt and Goode 2006). The emphasis, however, was placed on the so-called high-mast lighting poles, which are typically more than 100 ft in height and usually support multiple luminaires. The shorter poles, which usually support a single luminaire, are again not considered. In light of the recent occurrences of multiple failures of typical lighting poles (Caracoglia and Jones 2007), it appears that there is a need to study the mechanism of wind-induced vibrations of these seemingly simple structures and to reexamine the current design specifications.

This report summarizes the results of a full-scale investigation conducted under the sponsorship of Texas Department of Transportation (TxDOT) to understand the failure mechanisms of highway lighting poles. The goal of the research is to understand the "failure mechanisms of an aluminum light tower mounted on unoccupied signal foundation". This effort is part of the project "Revision of AASHTO Fatigue Design Loading for Signs, Luminaires and Traffic Signal Structures for Use in Texas" (Project No. 4586).

2   Technical Background

Potential excitation mechanisms for wind-induced lighting pole vibrations include vortex-shedding, buffeting and galloping. Vortex-induced vibration is caused by the periodic forces acting on a body when wind detaches from the body in the form of alternating vortices. The shedding frequencies of the vortices are controlled by the Strouhal relationship, which can be expressed as

$$\frac{N_s D}{U} = S \tag{1}$$

where D is the across-wind dimension of the body; U is the mean velocity of the flow; N_S is the shedding frequency of the vortices, also known as the Strouhal frequency, and S is the Strouhal number, which depends on body geometry and the Reynolds number (Simiu and Scanlan 1996). A key characteristic of vortex-induced vibration is the so-called phenomenon of "lock-in", whereas the mechanical frequency of a body controls the shedding of the vortices when it is close to (within several percent of) the nominal Strouhal frequency. At lock-in, the flow interacts strongly with the body, which creates steady oscillation with significant amplitude in the across-wind direction. This characteristic prescribes that large-amplitude vortex-induced vibration only occurs over a restricted range of wind speed for a given mode of a structure. The amplitude of vortex-induced vibration is self-limiting, since aerodynamic damping increases at higher oscillation amplitude.

Buffeting is an irregular motion of a structure or parts of a structure in a flow, excited by turbulence in the flow (Fung 2002). Buffeting has been observed to occur for line-like structures with low frequencies, such as slender towers or the decks of suspended-span bridges. Since buffeting is associated with the turbulence in the wind, for the same turbulence intensity, the response of the structure is usually larger at higher wind speeds.

Galloping is a type of oscillation experienced by an elastically sprung body, the frequency of whose main motion is low relative to its nominal vortex shedding frequency (Dowell and Crawley 1995). A classical type of galloping instability is the large-amplitude across-wind vibration of electric transmission lines coated with ice (Den Hartog 1956). Experience has proved that galloping is governed by quasi-steady forces. A quasi-static analytical model has led to the necessary condition for incipient galloping instability, which is the well-known Glauert-Den Hartog criterion (Den Hartog 1956) expressed as

$$(\frac{dC_L}{d\alpha} + C_D)_{\alpha=0} < 0 \tag{2}$$

where C_L and C_D are the lift and drag coefficients, respectively, of the oscillating body, and α is the angle of attack of the flow. For a circular cylinder positioned normal to direction of the flow, galloping cannot occur since the lift coefficient is constant around its circumference. Also, since turbulence can transform steady oscillation into unsteady ones and reduce the magnitude of aerodynamic damping, when the scale and intensity of the turbulence is high, it can destroy the necessary conditions for galloping (Simiu and Scanlan 1996).

This study will investigate the mechanism of wind-induced lighting pole vibrations by comparing the characteristics of such vibrations observed using a full-scale monitoring system with the known characteristics of the three types of vibration introduced herein.

3   Experiment Configuration

3.1   Subject of Study

The lighting poles subjected to investigation are a 40 ft cantilevered type made of aluminum. The manufacturer is the Union Metal Corporation. This type of lighting pole consists of a 35 ft tapering pole, which is 10 inches in outer diameter at the base and 6 inches in inner diameter at the top, and a cantilever arm that has a 12 ft spread and a 5.5 ft rise. The thickness of the pole is

0.188 inches. The cantilever arm is a bent aluminum tube of 0.125 inches in wall thickness. The horizontal portion of the arm has a circular cross-section of 2.375 inches in outer diameter. The inclined portion of the arm tapers from an elliptical cross-section (4.375 inches in outer major axis and 2.375 inches in outer minor axis) at the arm-pole connection to a circular cross-section of 2.375 inches in outer diameter where it terms horizontal. The arm is reinforced by an inclined aluminum strut of 1.5 inches in diameter and a vertical strut with an elliptical cross-section (1.5 inches in major axis and 0.675 inches in minor axis). The pole structure is designed to be anchored on a steel base, which is bolted to a concrete foundation. More details of the pole structure can be found in the shop drawings (provided by TxDOT) in Appendix A.

The poles monitored were erected according to standard procedures at the field test site at the Reese Technology Center, which is 8 miles away from the Texas Tech University campus in Lubbock, Texas. The first pole was installed in April 2006. It had to be dismantled within four months, however, due to wind-induced failure and damages to a number of connections between the structural members. For illustration purposes, Figure 1 (a) shows the failure of the connection between the pole and the cantilever arm, and Figure 1 (b) shows the damage to the welding between the pole and base plates. Since no monitoring system has been installed during the first several months of the project, the wind and the corresponding pole vibration that led to these failure and damages were not recorded. Based on the fact that the pole had been in service for a quite short period of time (Mr. Scott Walton, TxDOT, personal communications), however, it can be concluded that the failure and damages are due to extreme wind loading instead of fatigue of the structure members. After the failure of the first lighting pole, a second pole of the same type was installed at the same site in September 2006. This report will be based on interpretation of the observed vibrations of the second pole.
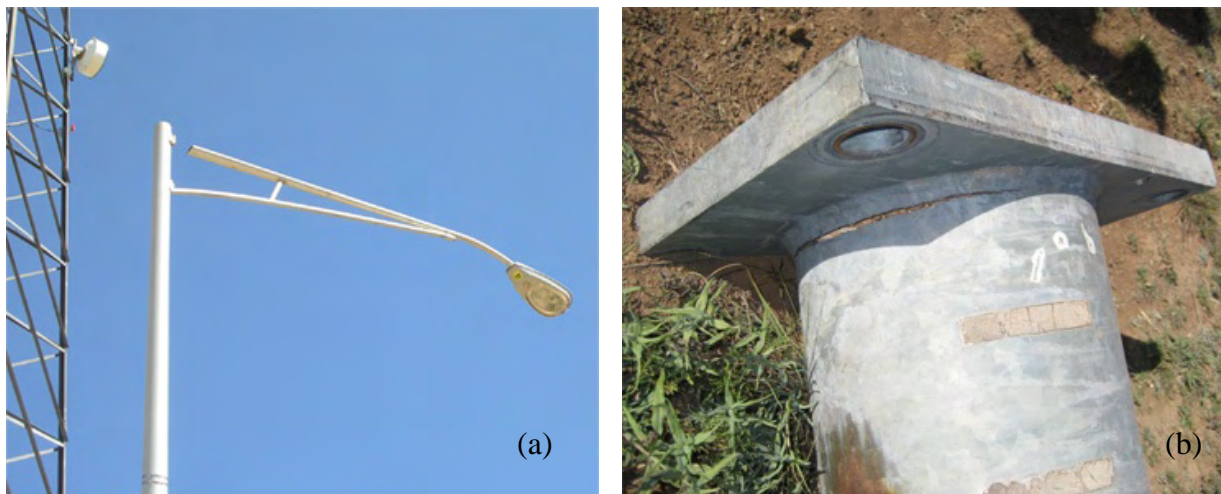
Figure 1 (a) Failure of the pole-arm connection; (b) damage to the pole-base plate connection

3.2   Monitoring System

To monitor the vibration of the pole, a displacement measurement system consisting of an infrared camera (Basler A601 video camera with National Instrument Compact Vision System 1454) and a target made of two infrared lights (Nerlite S-40) were installed on the structure. To measure the wind associated with the vibrations, an ultrasonic anemometer (R M Young

Company, model 8100; range: 0 to 40 m/s; resolution: 0.01 m/s; threshold: 0.01 m/s; output frequency: 4 to 32 Hz) was installed in the vicinity of the pole at a height of 13 feet about ground. In December 2006, tri-axial accelerometers (Crossbow Technology Inc., model CXL04LP3-R; capacity: $\pm 4g$; noise level: 10 mg) were installed at three different locations on the lighting pole structure: one at the top of the luminaire, one at the top tip of the pole and one at the 2/3 height of the pole. Figure 2 shows the second pole and the transducers used to monitor its vibrations and the corresponding wind. Measurements by all these transducers are continuously sampled at 30 Hz by a data acquisition system on an onsite computer. This data acquisition system records a data file every hour.

Figure 2 Forty feet lighting pole and the transducers used in monitoring

3.3 Coordinate System and Notation Conventions

As will be described in more detail subsequently, measurements by the monitoring system revealed that the vibrations of the pole can be highly three-dimensional. To characterize these complex vibrations in the context of the wind environment, a coordinate system is defined and illustrated in Figure 3. The direction along the axis of the cantilever arm, which points to the west, is designated the "X" direction; the direction perpendicular to the arm axis and pointing to the north is designated the "Y" direction; the vertically downwards direction is designated the "Z" direction according to the "right-hand rule" for Cartesian coordinates. With this coordinate system, the "X" and "Z" axes lie in the plane of the lighting pole structure formed by the pole and the cantilever arm. Vibration in this plane will be designated "in-plane". Accordingly, vibrations in the plane formed by the "Y" and "Z" axes will be designated "out-of-plane". To characterize the winds associated with the lighting pole vibrations, the angle between the wind direction and the vector pointing south, which is perpendicular to the axis of the lighting-pole arm, is designated the attack angle of the wind (θ). This attack angle is 0° when the wind approaches from the north, and it increases as the wind vector rotates clockwise. This scheme for characterization of wind direction relative to the lighting pole structure is shown in Figure 3.
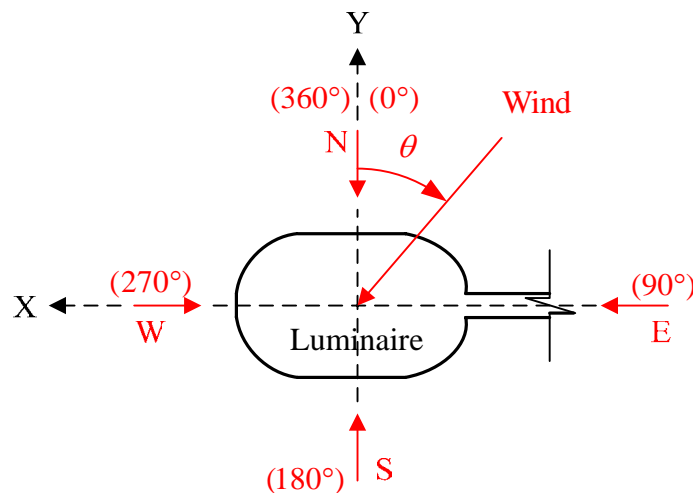
Figure 3 Coordinate system for characterization of lighting pole vibration in the context of wind

Since the oscillation of the pole is measured by three accelerometers at different locations, the conventions listed in Table 1 are introduced.

Table 1 Conventions used to characterize lighting pole vibration

Accelerometer Location	Acceleration	Displacement	Frequency
Top of Luminaire	Lumin acc	Lumin disp	Lumin freq
Top of Pole	Pole-U acc	Pole-U disp	Pole-U freq
2/3 Height of Pole	Pole-L acc	Pole-L disp	Pole-L freq

4 Data Processing

The results of the investigation presented in this report will be based on the lighting pole vibrations measured by the accelerometers and the wind speeds and directions measured by the ultrasonic anemometer. Since acceleration measurement inherently exaggerates the high frequency components in the vibrations, which can represent the unimportant higher modes in the vibration or simply undesirable noise, the acceleration time histories were numerically integrated twice to obtain the corresponding displacement time histories. To eliminate the low frequency noise that is magnified by the integration process, a sixth order high-pass Butterworth filter (Mitra 2004) was applied to the time histories after each step of integration. The cut-off frequencies of the filter are set as half of the natural frequencies of the fundamental modes in and out of the lighting pole plane. Figure 4 illustrates the result of numerical integration by showing a segment of acceleration time history recorded by the accelerometer at the top of the luminaire and the corresponding displacement time history obtained through numerical integration. It can be seen that most of the high-frequency oscillation components, which are pronounced in the acceleration signal, become invisible in the displacement time history, but the low-frequency component are apparent after the integration process.
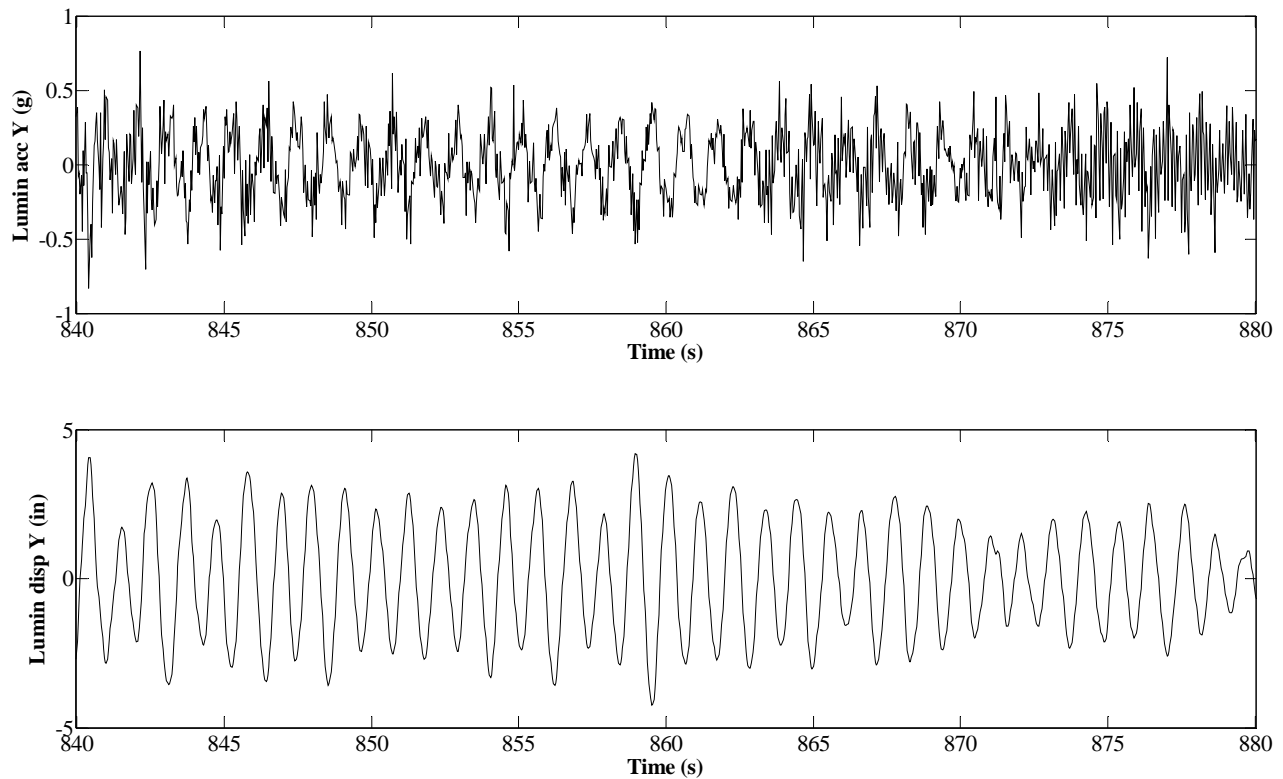
Figure 4 Example vibration segment illustrating the result of numerical integration

To analyze the vibration at the modal level, the first three modes of vibration in both the in-plane and out-of-plane directions were obtained by decomposing the displacement time histories using a sixth order band-pass Butterworth filter. For each mode, the pair of cut-off frequencies for the Butterworth filter were chosen to be 0.33 Hz (which is approximately one third of the fundamental frequencies of the pole in the in-plane and out-of plane directions) below and above

the frequency of this mode. The modal frequencies of the lighting pole were identified by analyzing the power spectral density functions of the vibrations estimated based on the acceleration time histories measured by the accelerometers. This procedure will be described in the subsequent section. To simultaneously estimate the instantaneous amplitude and frequency of vibration at a specific time, the modal displacement time histories obtained by band-pass filtering were subjected to the Hilbert transform (Bendat and Piersol 2000). Figure 5 shows the time history of the first-mode vibration decomposed from the displacement time history shown in Figure 4 and the estimated instantaneous amplitudes and frequencies. It can be observed that for this particular segment, the vibration of the luminaire in the Y direction was primarily in the first out-of-plane mode of the structure. It also can be seen that the Hilbert transform has faithfully preserved the amplitude of the modal vibration. The fluctuation of the vibration frequency is believe to be due to the fluctuation of the primary loading frequency in the proximity of the natural frequency of the structure in this mode. The natural frequency of this mode, therefore, can be estimated as the mean value of this fluctuating frequency.
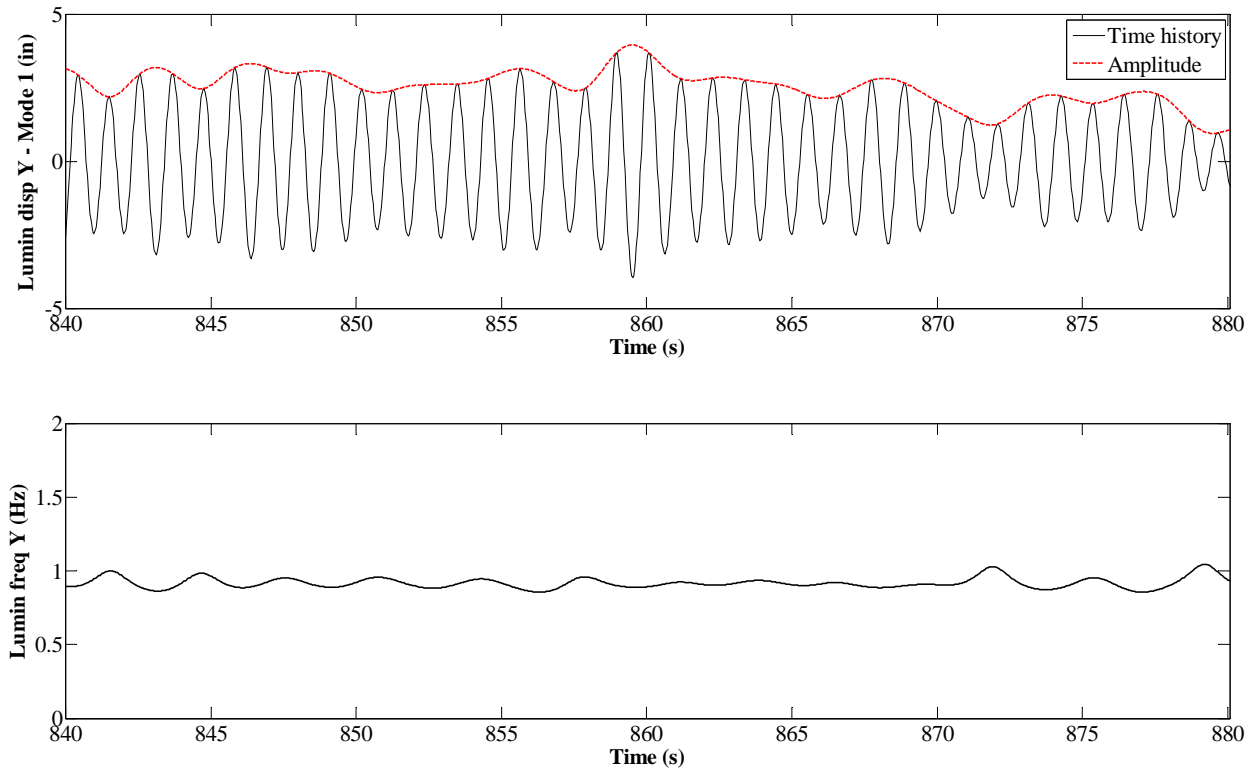
Figure 5 Example modal vibration segment illustrating the result of Hilbert transform

5   Modal Analysis

Numerical simulation based on finite element method (FEM) and spectral analysis of the full-scale measurement data were incorporated in this study to identify the mode shapes and modal frequencies of the lighting pole structure. To assess the damping ratios in the modes of interest, manually forced vibration tests were conducted and the resulting free-decay vibration data were analyzed using the logarithmic decrement method.

5.1 Mode Shape and Frequency Estimation

The FEM model for the lighting pole structure was developed using the commercial software SAP2000. Beam elements were used to model the pole, the arm and the struts; the luminaire was modeled as a concentrated mass; the anchorage system was modeled as a fixed support. Figure 6 depicts the shapes of the first six natural modes of the structure. The corresponding modal frequencies are also listed. As can be seen in the figure and as suggested earlier, the in-plane modes are in the plane formed by the X and Z axes; the out-of-plane modes are in the plane formed by the Y and Z axes. All the modes shown are bending modes of the structure. Since the frequencies of the torsional modes are high, they are not of primary interest for dynamic analysis and therefore not included in Figure 6. It must be noted that although the mode shapes of the first and second out-of-plane modes appear to be similar, this is due to a false representation by the graphs since they cannot effectively depict the bending of the cantilever arm.

1st in-plane mode
$f_{xz,1} = 1.17$ Hz

2nd in-plane mode
$f_{xz,2} = 3.30$ Hz

3rd in-plane mode
$f_{xz,2} = 9.73$ Hz

1st out-of-plane mode
$f_{yz,1} = 0.91$ Hz

2nd out-of-plane mode
$f_{yz,1} = 2.60$ Hz

3rd out-of-plane mode
$f_{yz,1} = 10.01$ Hz

Figure 6 Mode shapes and modal frequencies of the lower modes estimated using FEM model

Since the finite element method is inherently an approximate approach, the measured data were also used to estimate the modal frequencies of the structure. Figure 7 and Figure 8 depict the time histories and the corresponding power spectra density functions of the luminaire vibration in the X, Y, and Z directions for an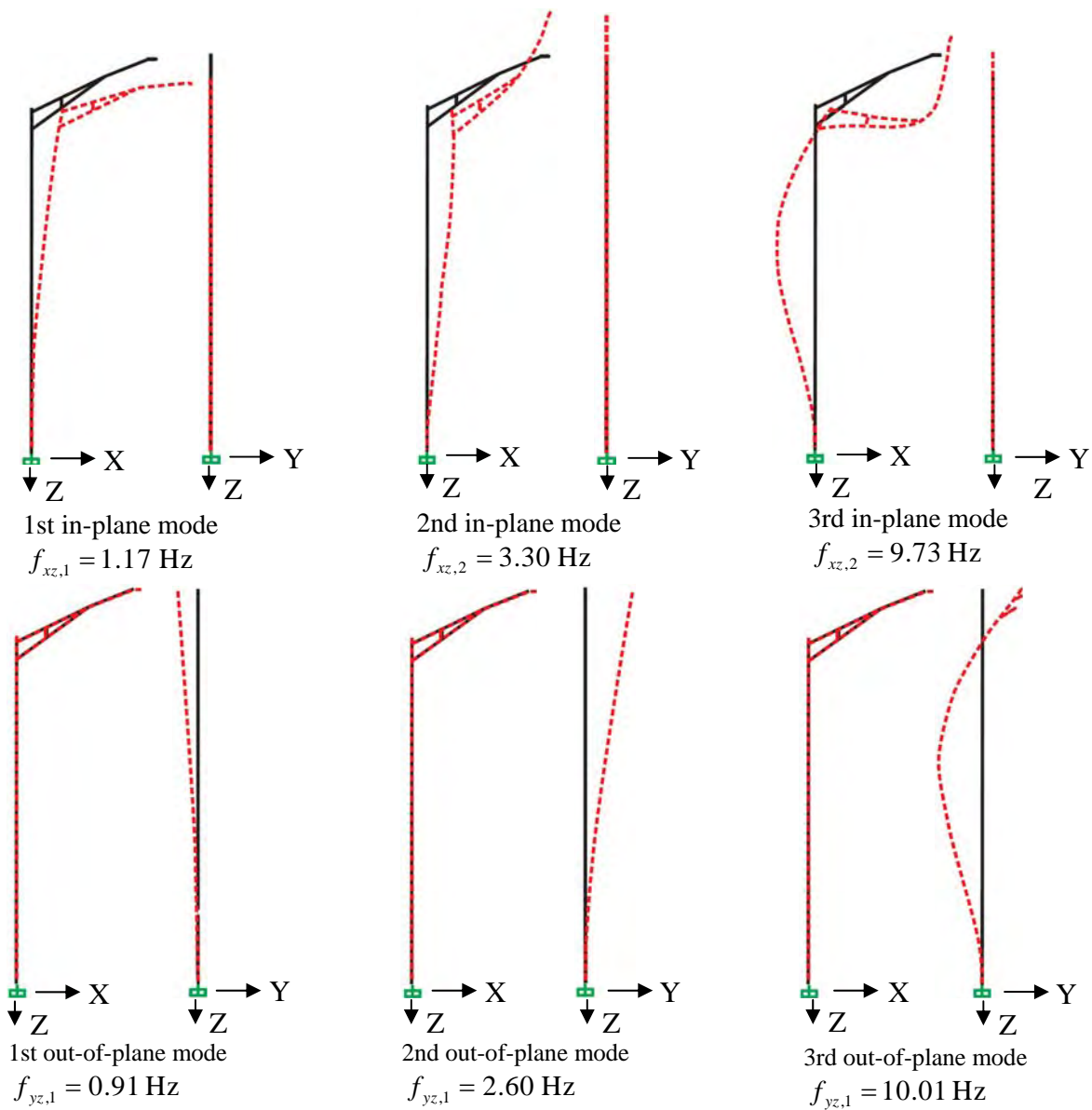 example one-hour record. Although the vibrations components were not stationary, the power spectral density functions can still be used for estimation of the frequency characteristics of the vibration. Since the frequency domain transfer functions for the lighting pole structure are essentially band-pass filters with cut-off frequencies close to the natural frequencies of the structure, the peaks in the power spectral density functions represent the response of the structure at frequencies close to these natural frequencies. Identification of these frequencies associated with these peaks, therefore, enables a reasonable estimation of the natural frequencies of the structure. According to Figure 8, the frequencies of the first three in-plane mode are 1.13 Hz, 3.60 Hz and 9.34 Hz, respectively; the frequencies of the first out-of-plane modes are 0.91 Hz, 2.71 Hz and 8.95 Hz, respectively. It can be seen that the in-plane modes appear in the X and Z directions only and that the out-of-plane modes appear in the Y direction only. A special case is the vibration of the luminaire in the second in-plane mode: While it appears to be a significant component in the Z direction, it is practically undetectable in the X direction. This is because this particular mode shape does have a strong vertical component but negligible along-arm component at the luminaire location, as shown in Figure 6. This situation is reversed at the upper end of the pole. Figure 9 shows the power spectral density functions of the vibration at this location during the same period of time. It can be seen that at the top of the pole, the second mode vibration is a strong component in the X direction but not detectable in the Z direction.
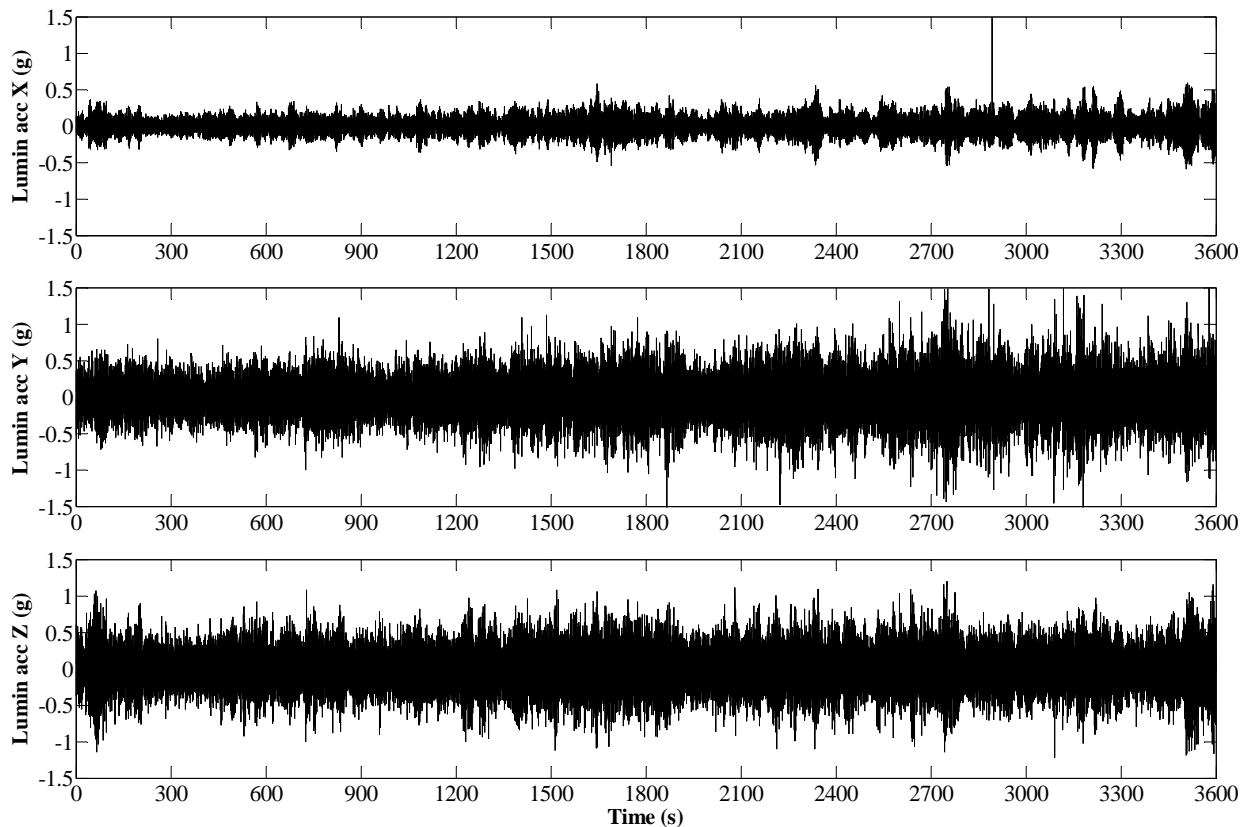

Figure 7 Acceleration time histories of luminaire vibration for an example record
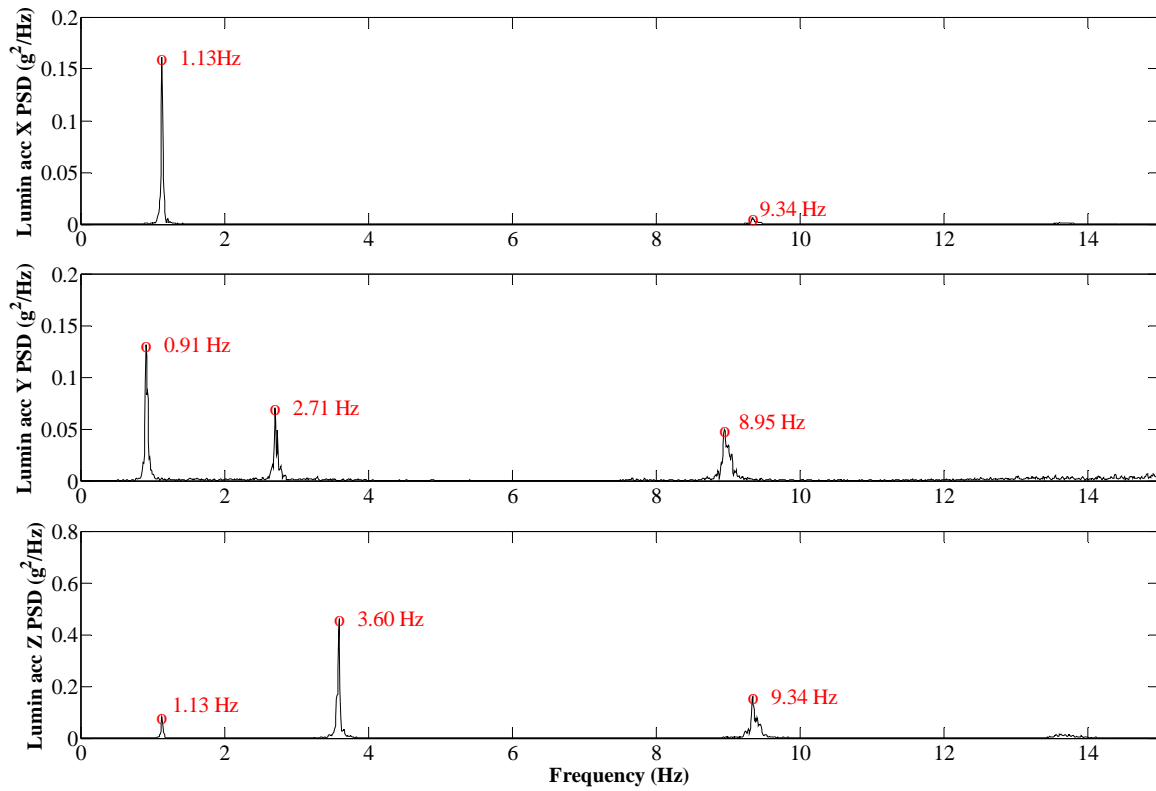
Figure 8 Power spectral density functions of the luminaire acceleration shown in Figure 7
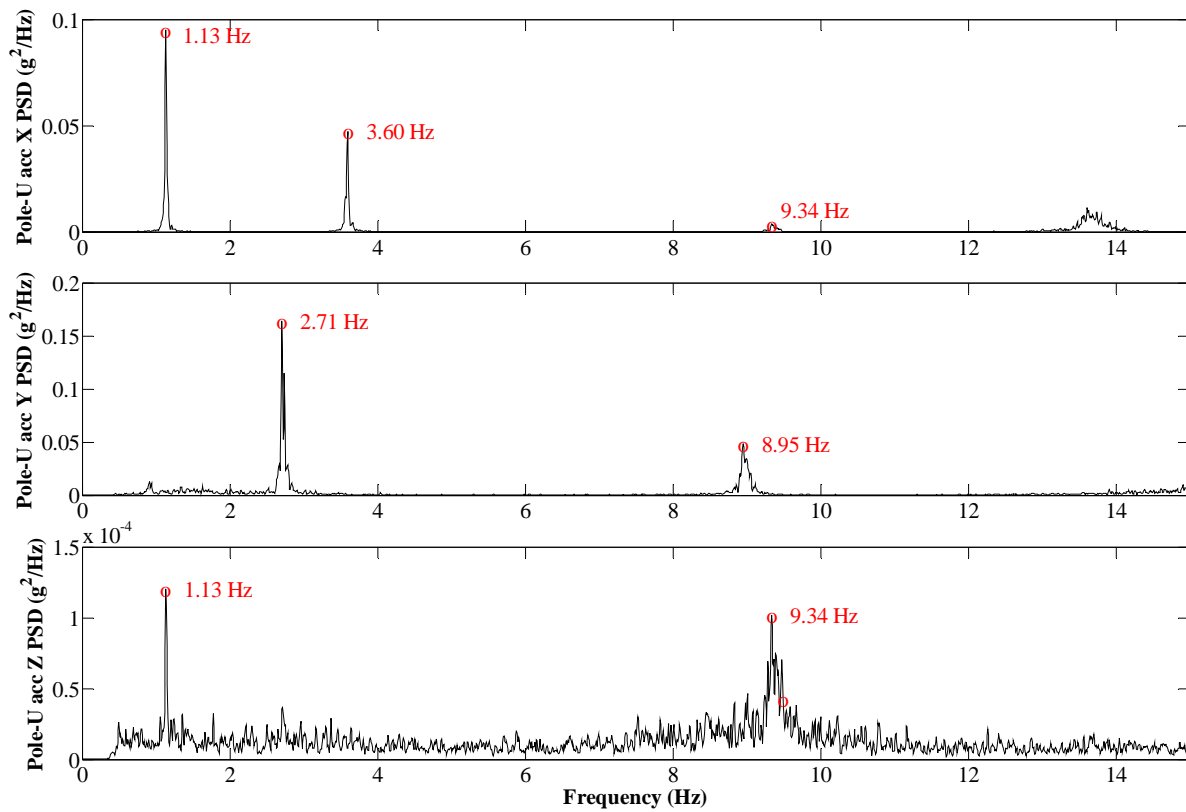

Figure 9 Power spectral density functions of pole-top acceleration

Table 2 lists the frequency estimates based on the FEM approach and spectral analysis approach (average of multiple estimations, which coincidentally is in agreement with the values shown in Figure 8 and Figure 9). It can be seen that the modal frequencies estimated using these two approaches are very close for the first two in-plane and out-of-plane modes. For the third modes in these two planes, however, the results of numerical simulation (9.73 Hz in-plane, 10.01 Hz lateral) are quite different from those of spectral analysis (9.34 Hz in-plane, 8.95 Hz lateral). This is believed to be due to the fact that the higher modes are sensitive to the detailed structural configuration which the FEM model does not adequately represent.

Table 2 Estimated natural frequencies of the first three in-plane and out-of-plane modes

Mode	1st In-Plane	1st Out-of-Plane	2nd In-Plane	2nd Out-of-Plane	3rd In-Plane	3rd Out-of-Plane
FEM	1.17 Hz	0.91 Hz	3.30 Hz	2.60 Hz	9.73 Hz	10.01 Hz
Full-Scale	1.13 Hz	0.91 Hz	3.60 Hz	2.70 Hz	9.34 Hz	8.95 Hz

A specific characteristic of these modal properties of this lighting pole is that its modal frequencies in the in-plane and out-of-plane directions are fully uncoupled. This, as will be described subsequently, has significantly affected the response of the structure to wind excitation.

5.2   Damping Estimation

To assess the inherent mechanical damping in the lighting pole structure, a series of manually forced vibration tests were conducted to facilitate free-vibration data needed for the application of the logarithmic decrement method, which is briefly introduced subsequently. During the tests, a rope was tied to the pole at a distance of about 20 feet (half of the pole height) from the anchorage. The rope was then pulled at frequencies close to the pre-identified nature frequencies of the structure to force the lighting pole to vibrate in the modes of interest. When the forced vibration reached sufficiently large amplitude, the rope was released to allow the vibration to decay freely. Such pull-and-release procedures were applied in both the in-plane and out-of-plane directions (approximately) so that the damping ratios of the modes in both planes of the structure can be assessed. Due to the difficulty involved in exciting the higher modes of the structure, the tests were conducted only for the first in-plane and out-of-plane modes. The tests were chosen to be performed under low wind speeds (about 5 miles per hour) so that the aerodynamic damping can be neglected. This section will use two examples to illustrate the damping in the first in-plane and out-of-plane modes of the structure.

Figure 10 shows representative in-plane vibration components during the forced vibration tests that spanned a one-hour period. These time histories were obtained using the numerical integration procedure described earlier. The components "Lumin X" and "Lumin Z" and "Pole-U X" were chosen for analysis because the measurements by the accelerometers reached the largest amplitude according to the shape of the first in-plane mode (Figure 6). As shown in the time histories, three in-plane tests were conducted between the 900th and the 1800th seconds of the record. The moderate-amplitude vibrations starting from approximately the 2400th second were due to the out-of-plane tests, since it was practically impossible to force vibration in only one plane.
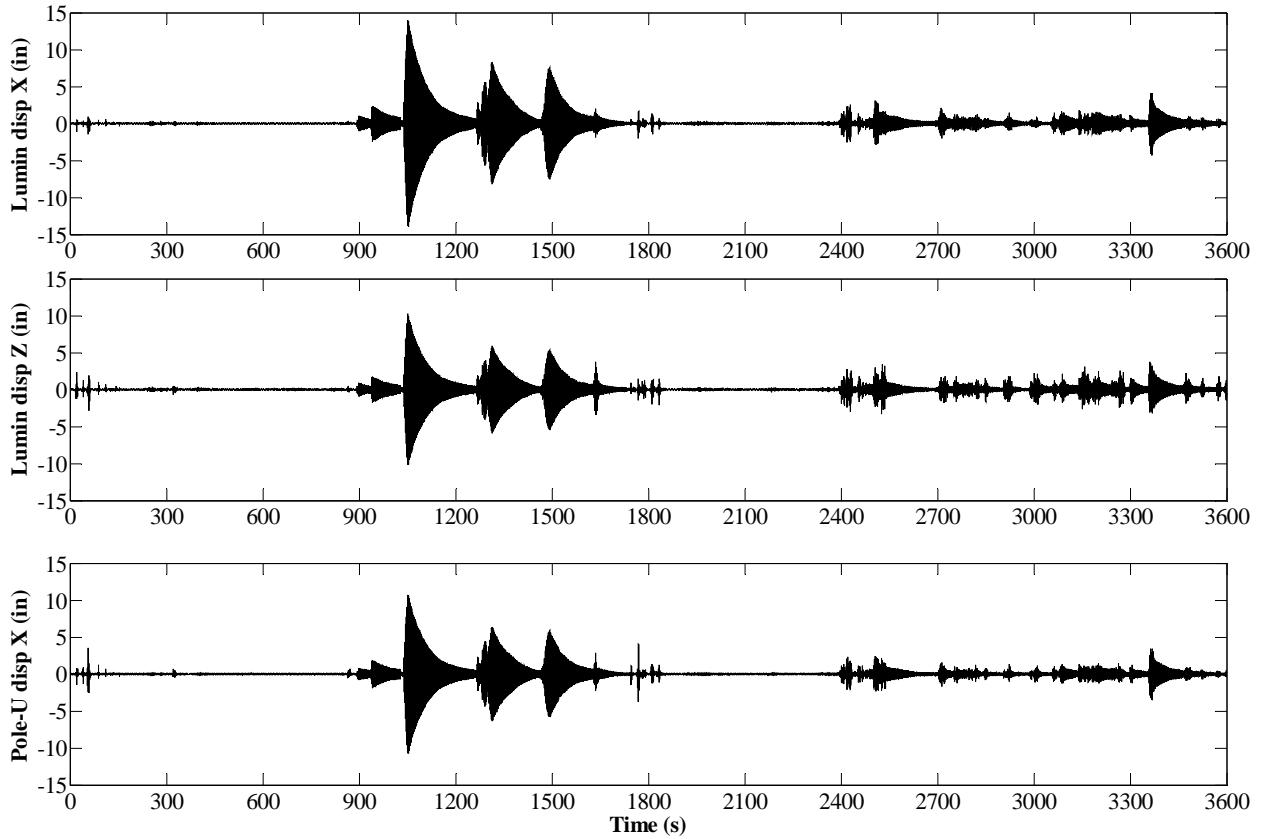
18

Figure 10 Displacement time histories showing manually forced in-plane vibration

Although the responses of the pole were primarily in the modes whose frequencies are close to the pulling frequencies, some other modes were also excited simultaneously and, as a result, exhibited insignificant oscillations. A sixth-order band-pass Butterworth filter was therefore applied to obtain the vibrations in the modes of vibration only. For illustration purposes, Figure 11 depicts a segment of the first in-plane mode vibrations decomposed from the displacements shown in Figure 10, together with the identified peaks of the vibrations.

According to the logarithmic decrement method (Clough and Penzien 2003), if the damping ratio in a mode of vibration is small (e.g., less than 20%), it can be expressed as

$$\zeta = \frac{\delta}{2\pi}; \quad \delta = \ln \frac{x_i}{x_{i+1}} \tag{3}$$

where δ is the so-called logarithmic decrement of the free modal vibration; x_i and x_{i+1} are two successive peaks of the vibration. In this study, the logarithmic decrement method was applied progressively for the peaks. For every five peaks, the average of the four damping ratios estimated is taken as the representative damping ratio during the sub-segment of vibration containing these five peaks. Accordingly, the displacement of the third peak was taken as the representative amplitude. This scheme enabled an assessment of the amplitude dependent nature of the damping in the structure. As an example, Figure 12 presents the average damping ratios estimated based on the segments shown in Figure 11 against the corresponding representative amplitudes. It is apparent that the level of damping in the first in-plane mode of the lighting pole is very low. It is also evident that the damping in the first in-plane mode of the structure depends

strongly on the vibration amplitude: when the amplitude is low, the average damping ratio increases with the amplitude of the displacement. When the amplitude reaches a specific level (for example, about 3 inches in the X direction at location of the luminaire), the average damping ratio reaches a plateau and stays at the same level. This vibration amplitude dependent nature of the modal damping is important for the interaction between the lighting pole and the wind. For many aeroelastic phenomena, the level of damping ratio at low vibration amplitude controls the onset of problematic vibration, and the level of damping ratio at higher amplitudes determines the largest attainable amplitude of the vibration.

Figure 11 A segment of vibration in the first in-plane mode
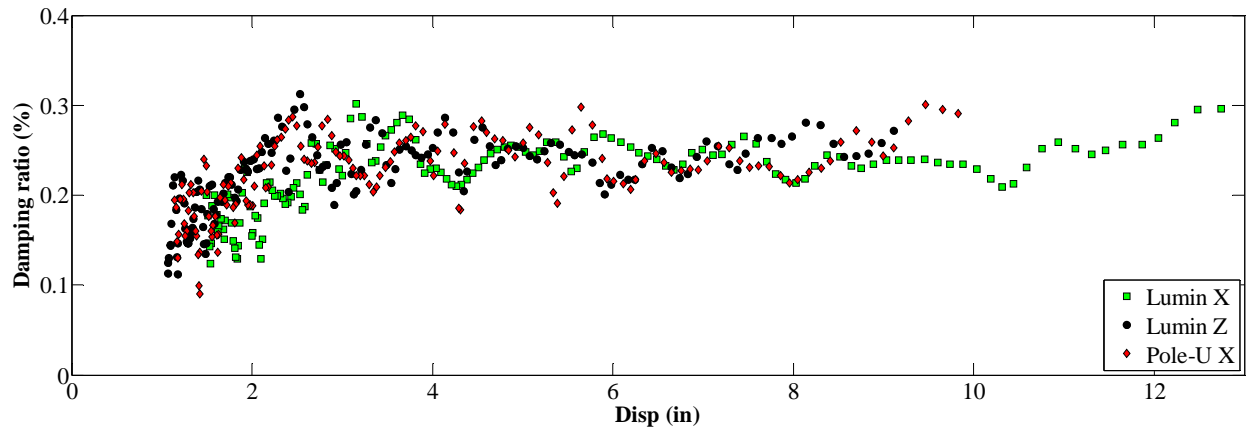
Figure 12 Estimated damping ratio in the first in-plane mode from an example test

Figure 13 shows the representative out-of-plane vibration components during the forced vibration tests that spanned a one-hour period. The out-of-plane tests were conducted between the 2700th and the 3600th seconds. Figure 14 depicts a segment of the first out-of-plane mode vibrations decomposed from the time histories shown in Figure 13 together with the identified peaks of the vibrations. Figure 15 presents the result of damping estimation using the logarithmic decrement method. It appears that the damping in the first out-of-plane mode also depends on the vibration amplitude: the level of damping is low at low vibration amplitude, but increases to a relatively high level when the amplitude increases. By comparing Figure 12 and Figure 15, it is also apparent that the damping in the first out-of-plane mode is at a considerably higher level than that in the first in-plane mode. This is especially true when the amplitude of the vibration is high.

Figure 13 Displacement time histories showing manually forced in-plane vibration
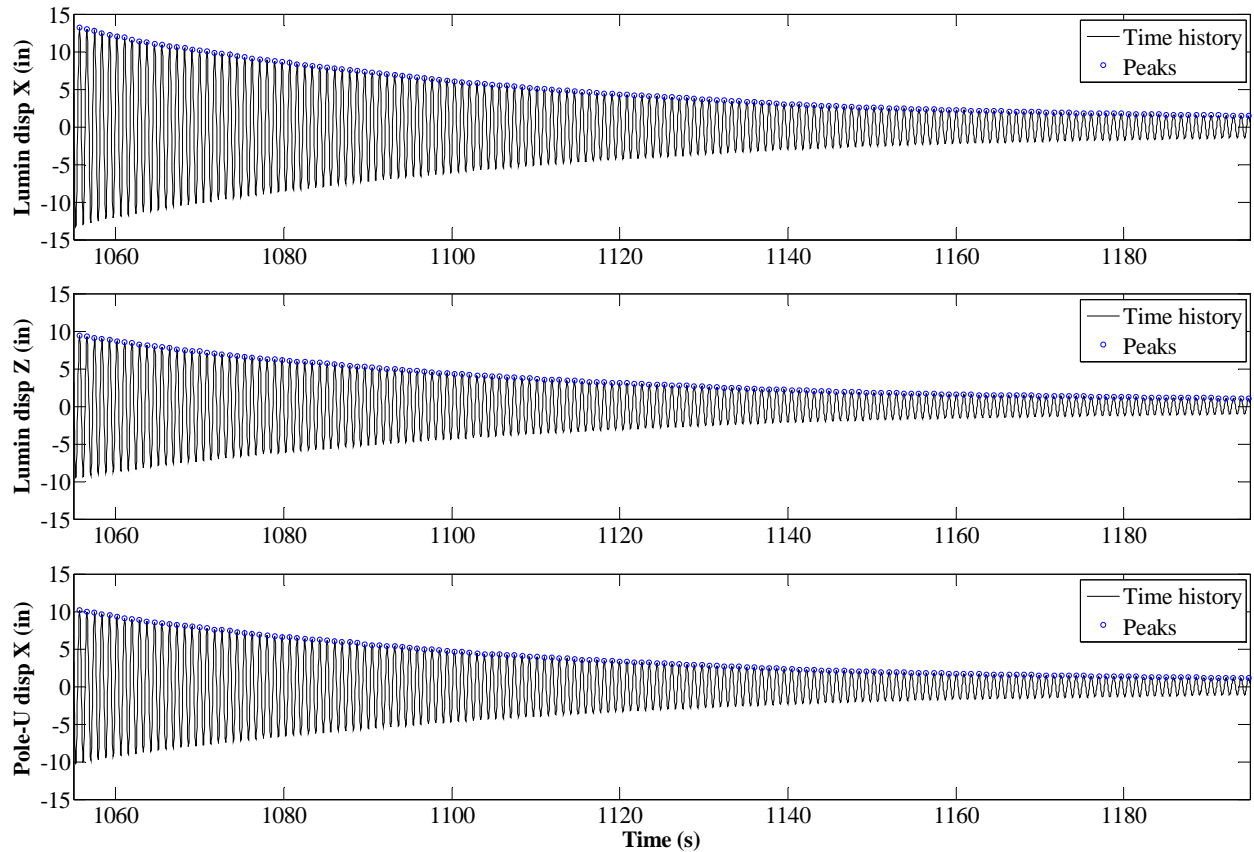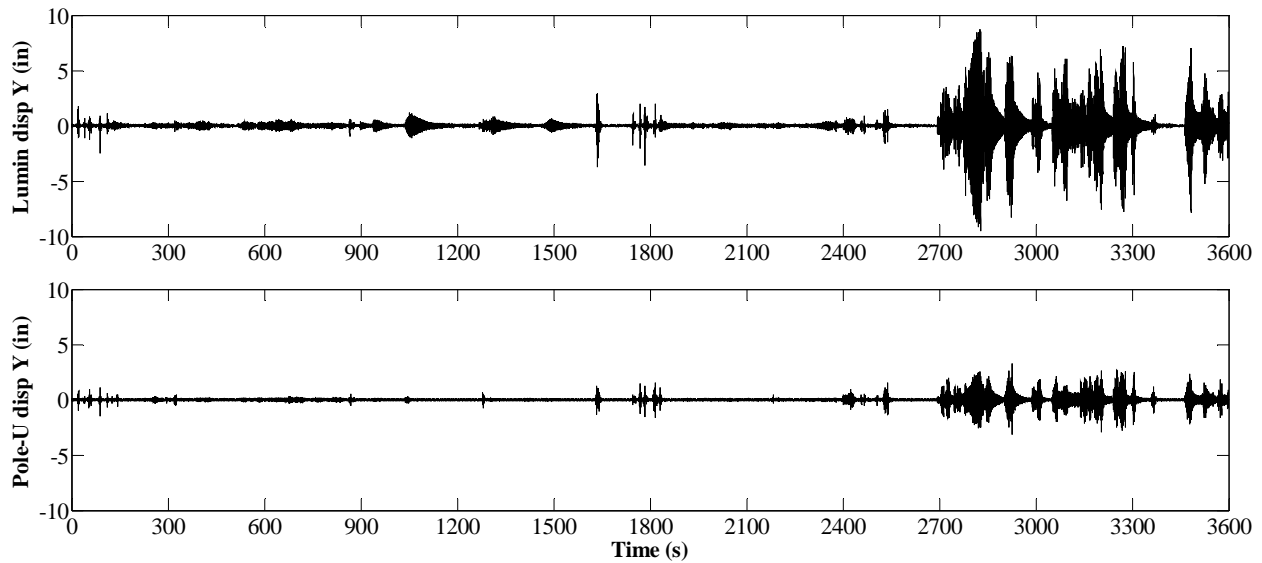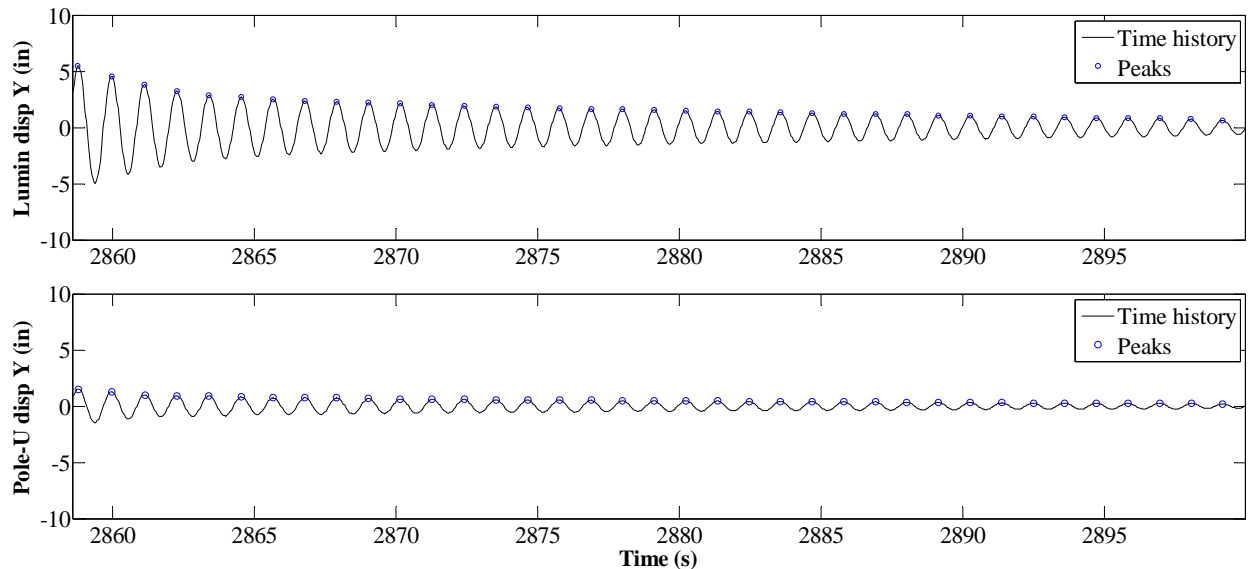

Figure 14 A segment of vibration in the first out-of-plane mode
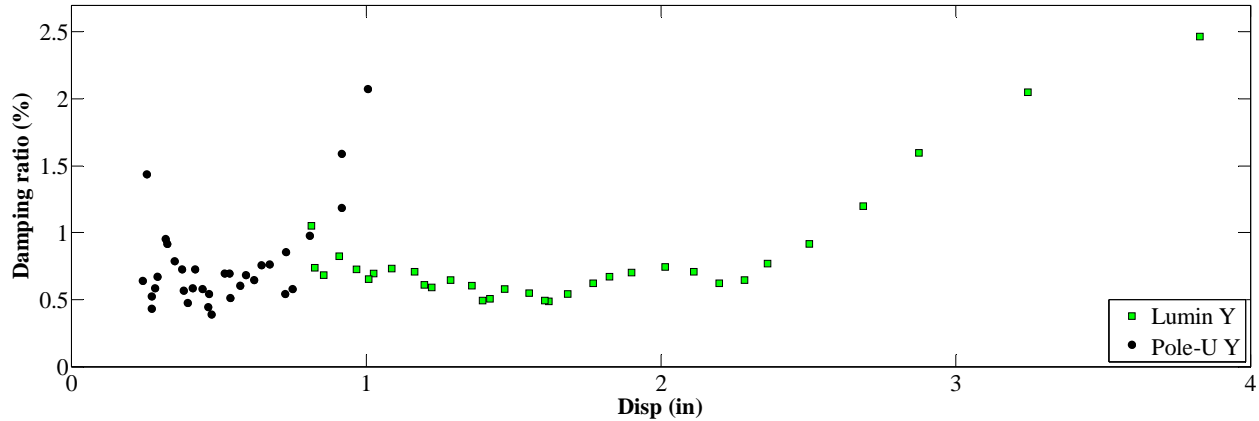
Figure 15 Estimated damping ratio in the first out-of-plane mode from an example test

Similar characteristics were observed for the damping in the first in-plane and out-of-plane modes based on other runs in the series of manually forced vibration tests. For brevity, results based on these tests are not presented herein.

6   Interpretation of Observed Vibrations

As will be described in more detail subsequently, most of the large-amplitude lighting-pole vibrations were highly nonlinear. For to this reason, the one-hour time histories were divided into 30-second segments to enable statistical analysis of the correlation between the wind and the resultant vibrations with adequate resolution.

During the course of the full-scale measurement project (from January to October 2007), winds of broad ranges of direction, speed and turbulence intensity were recorded. This is illustrated by the wind direction roses shown in Figure 16 for three ranges of wind speed, as well as the histogram of the wind speed and the turbulence intensity shown in Figure 17. This broad variation of wind provided a good context for the study of the vibration mechanisms. This chapter presents an interpretation of the general characteristics of the lighting pole vibrations and their correlation with wind and, based on this interpretation, an investigation of the vibration mechanisms at the modal level.

Wind speed < 10 mph   10 mph < Wind speed < 20 mph   Wind speed > 20 mph

Figure 16 Rose of wind directions recorded during the monitoring program

Figure 17 Histogram of speed and turbulence intensity of winds recorded

6.1 Interpretation of General Characteristics of the Vibrations

The full-scale data have revealed some key characteristics of the lighting pole vibrations. This section presents an interpretation of these characteristics in the context of the wind environment.
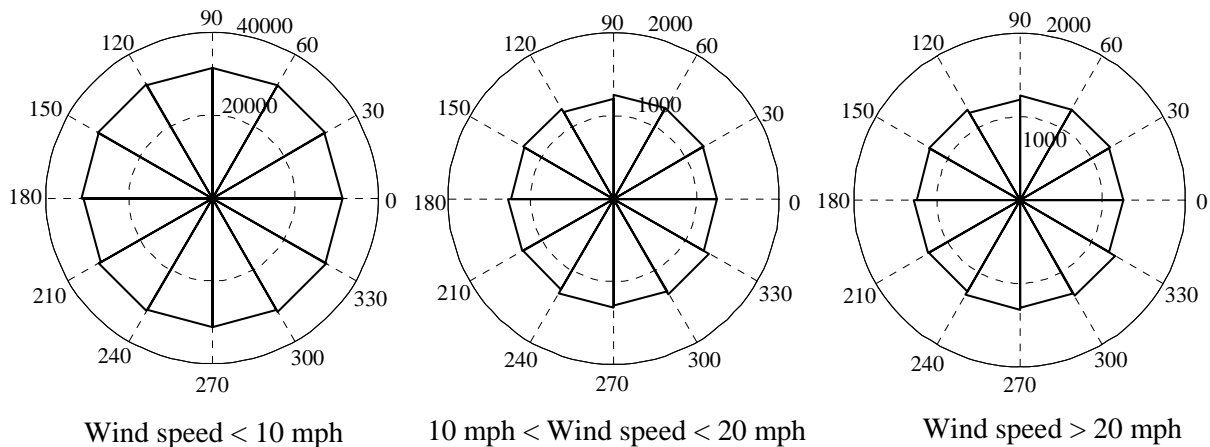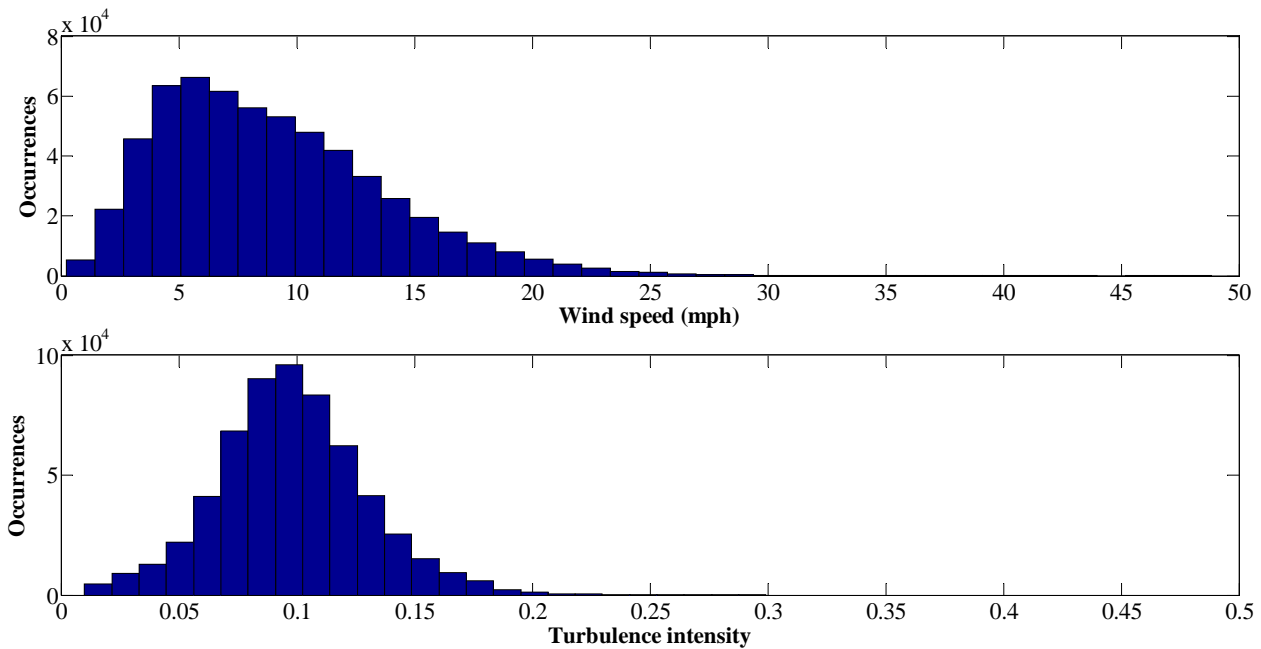
To investigate the effects of wind speed on the vibrations, the 30-second statistics were organized into 12 groups according to wind direction range. Each group contains data associated with wind direction (θ) ranging over a 30° span. Figure 18 shows the root-mean-square (RMS) in-plane (X) and out-of-plane (Y) vibration amplitudes of the upper pole tip versus wind speed for these 12 groups of data. Only vibration segments with RMS amplitude greater than 0.1 inches in either direction are included. Since the Z component of the vibrations is inherently at a low level at this location, it is not shown herein to enable better clarity of the graphs. Two categories of vibration can be identified, both depending strongly on wind speed. Category one corresponds to clusters A in the graphs for all wind direction ranges. The amplitudes of this category of vibration in both directions were low at low wind speed, but increased with wind speed and reach a quite high level at high wind speeds. This type of correlation between vibration amplitude and wind speed is a known characteristic of galloping and buffeting-induced vibration (Simiu and Scanlan 1996). Category two corresponds to clusters B in the graphs associated with direction ranges of 60° to 120° and 240° to 300°. For this category, the out-of-plane amplitudes reached a moderate level over a narrow wind speed range (about 4 mph to 10 mph). As introduced in Chapter 2, this wind-speed-restricted nature is a characteristic of vortex-induced vibration. This type of vibration is not present in the graphs for vibrations in the in-plane (X) direction. This is because, as will be described later, they occurred in the second in-plane mode of the structure, whose shape (Figure 6) prescribes that the vibration amplitude at the location of the upper pole tip be low compared to, for example, the amplitude in the Z direction (also in-plane) at the luminaire location. The second category of vibration did occur in the in-plane direction and this will be demonstrated in the next section.
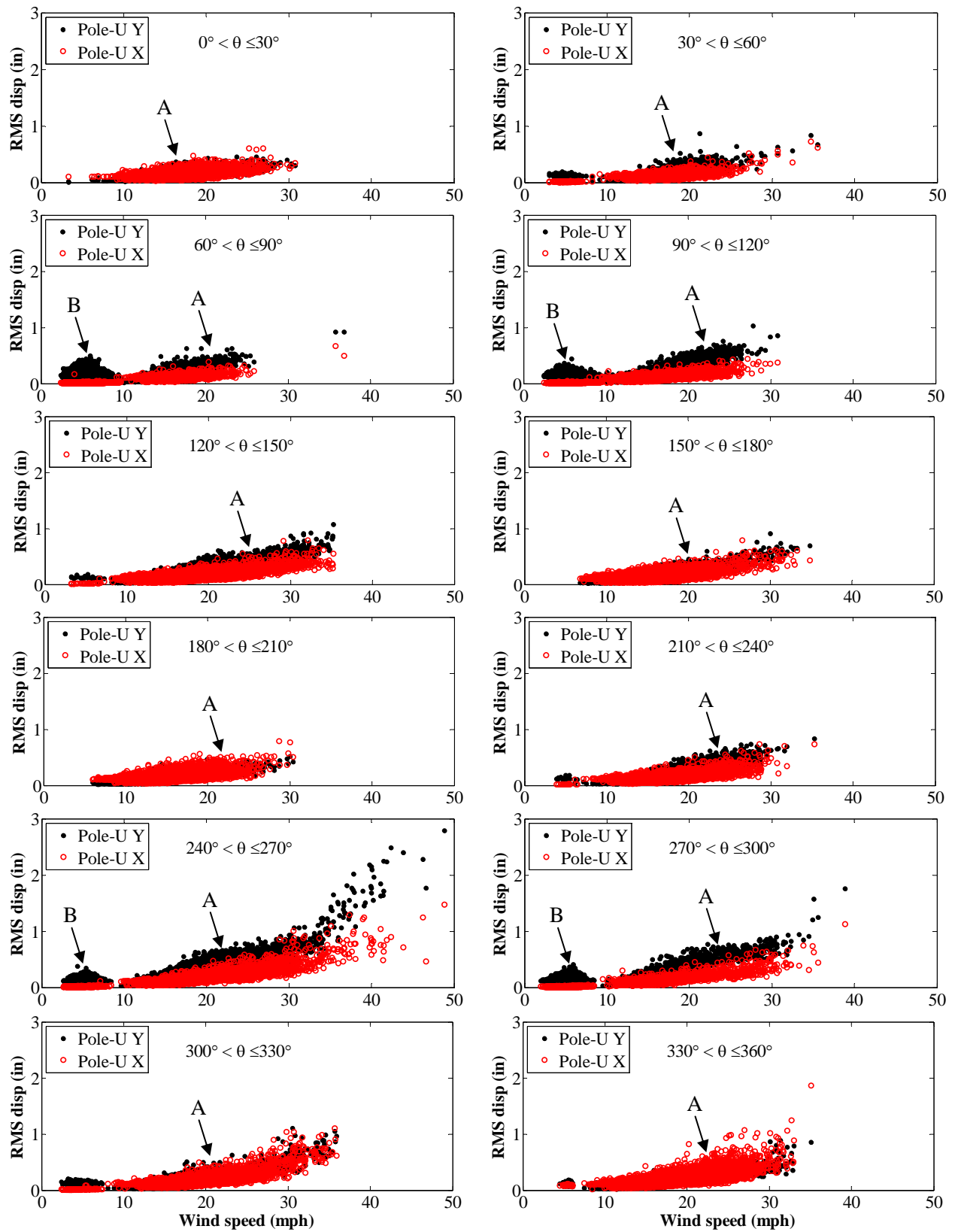
Figure 18 Correlation between vibration amplitude and wind speed for different wind directions

To investigate the dependence of the vibrations on wind direction, the 30-second statistics were organized into six groups according to wind speed range. Figure 19 presents the RMS displacement amplitudes against wind directions for these six groups of data. The data associated with wind speed greater than 10 mph in the graphs of Figure 19 are all associated with first category of vibration clusters "A" shown in Figure 18. This category of vibration does not appear to have a clear dependence on wind direction. Vibrations in category two shown in Figure 18 as clusters "B" are identified as the two clusters of out-of-plane vibration with moderate RMS amplitude centered at wind directions of 90° and 270° in the graph associated with wind speed range of less than 10 mph. This confirms the observation that this type of vibration has a strong dependence on wind direction.
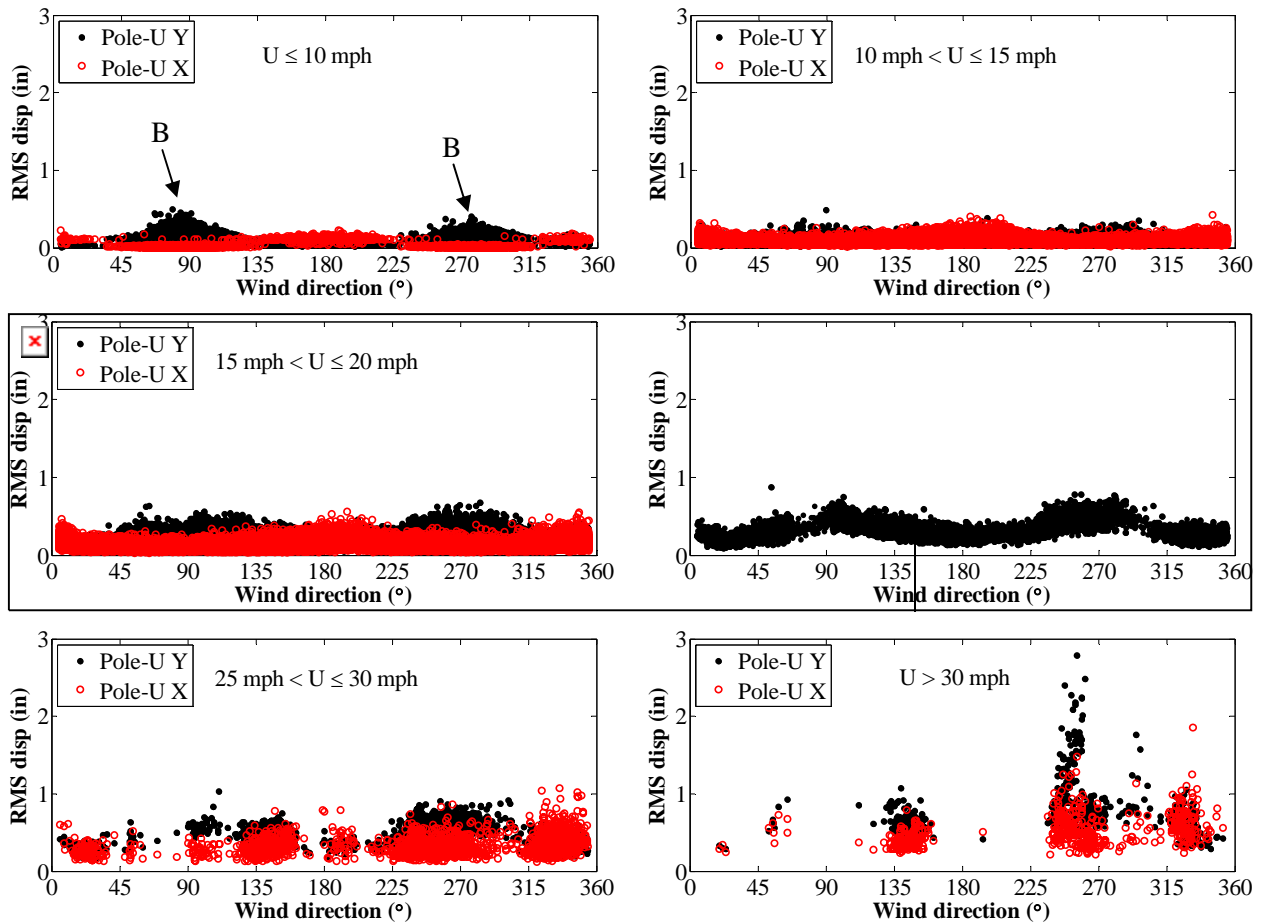
Figure 19 Correlation between vibration amplitude and wind direction for different wind speeds

This particular wind-direction-dependent nature of the vibrations in category two, which will be proved subsequently to be vortex-induced, is due to the fact that the frequencies of many in-plane and out-of plane modes of the lighting pole are substantially different (Table 2). This makes it impossible for the vortex-shedding frequency to be simultaneously locked-in with both the frequency of an in-plane mode and that of an out-of-plane mode. The only possible type of vortex-induced vibration, therefore, must be predominantly in either the in-plane or the out-of-plane direction of the lighting pole. This, and the fact that large-amplitude vortex-induced vibration is predominantly in the across-wind direction, decides that for lock-in to occur, wind

must approach in the in-plane direction to cause out-of-plane vortex-induced vibration, or the out-of-plane direction to create in-plane vibration. For example, for the second category of vibration shown in Figure 18 and Figure 19, the vibrations were in the out-of-plane (Y) direction, while the wind direction of 90° and 270° are in the in-plane (X) direction of the lighting pole.

This single-planar nature of the vibration in the second category can also be observed in the statistical spatial correlations between the components of the observed vibrations. Figure 20 shows this correlation for the vibrations at the upper pole tip location. It is confirmed by these graphs that the vibrations in this category are always predominantly in the Y direction. Figure 21 shows the spatial correlation of the vibrations in the second category at the luminaire location. The in-plane vibrations are primarily represented by the component in the Z direction, since the shape of the second in-plane mode (which is the mode in which the in-plane vibrations in this category occurred) inherently restricts the vibration in the X direction (Figure 6). It can be seen that vibrations were either predominantly in the in-plane (Z) direction or the out-of-plane (Y) direction at the luminaire location. No significant coupling of the in-plane and out-of-plane vibrations was present. Only vibrations with RMS amplitude greater than 0.2 inches are included in Figure 20 and Figure 21 to ensure that only data in the second category are presented.

Figure 20 Statistical spatial correlation of vibrations in category two at the upper pole tip
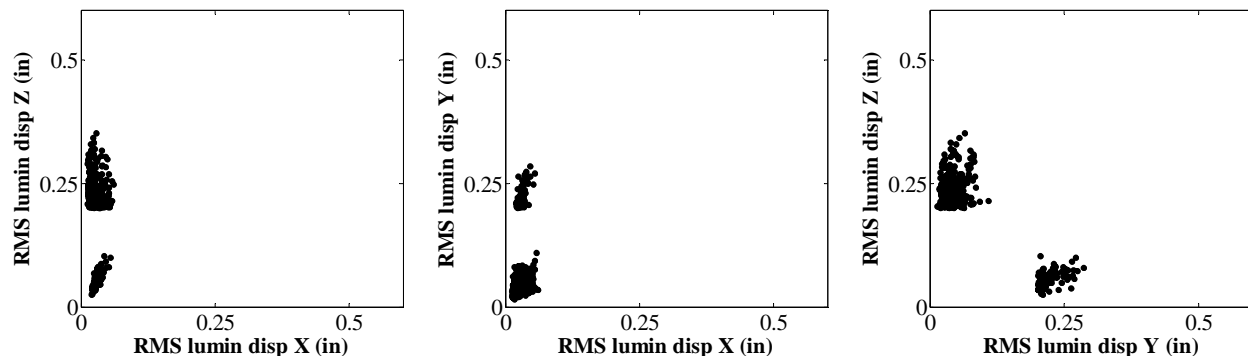
Figure 21 Statistical spatial correlation of vibrations in category two at the luminaire

For comparison, Figure 22 and Figure 23 present the spatial correlations for the vibrations in category one at the upper pole tip location and at the luminaire location, respectively. It is apparent that for this category, most of the vibrations at the upper pole tip were highly two dimensional, involving coupling of the in-plane and out-of-plane directions and those of the luminaire were highly three-dimensional. Again, the vibrations in the Z direction were restrained

by the high vertical rigidity of the pole. This characteristic suggests that the vibrations in category one was likely not induced by galloping instability, since galloping of structures are often dominated by across-wind response. It is suspected, therefore, that this category of vibration was induced by buffeting.

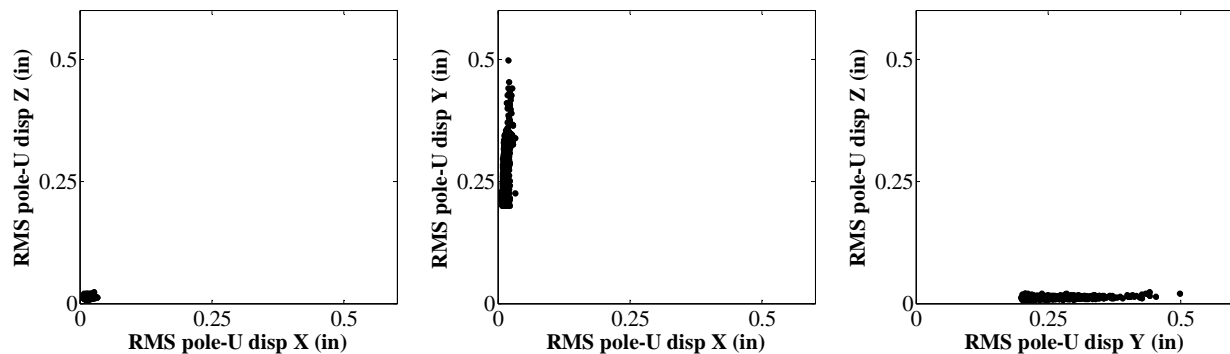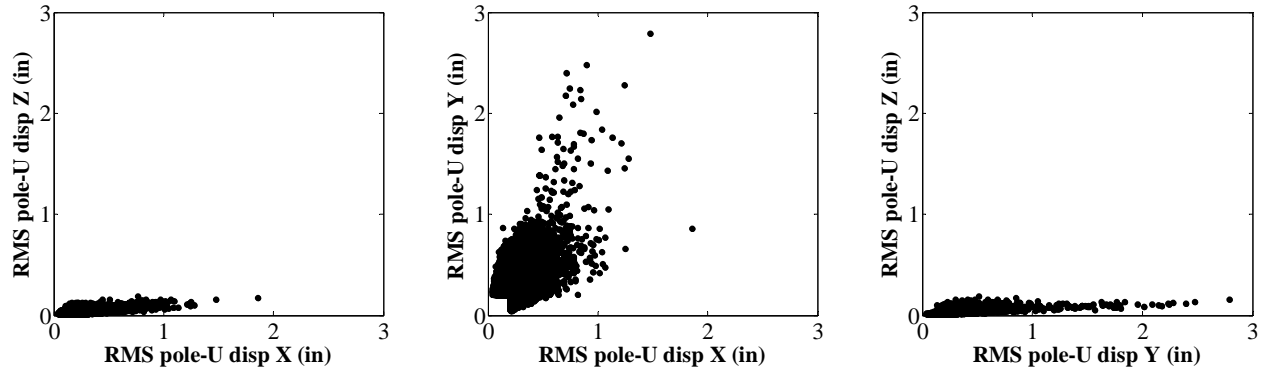Figure 22 spatial correlation of vibrations in category one at the upper pole tip
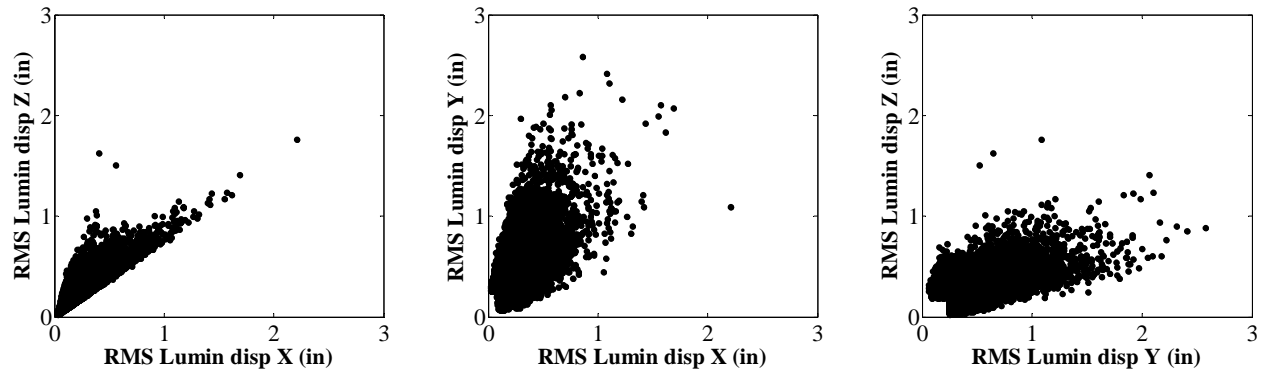
Figure 23 Spatial correlation of vibrations in category one at the luminaire

Another significant difference between the two categories of vibrations is that those in category two were usually steady and those in category one were often unsteady. As an example, Figure 24 shows the displacement time histories of a 2-minute vibration segment from a record in category one and Figure 25 shows those of an unsteady vibration segment in the category one. The difference in the steadiness of the vibrations is apparent. These records also illustrate again that the vibrations in category two were predominantly in one plane and that the vibrations in category one involved coupling of the in-plane and out-of-plane components. Figure 26 shows the wind speed and direction associated with the unsteady vibrations shown in Figure 25. It can be seen that the mean wind speed and direction were both considerably constant, but the turbulence in the wind had changed with time. The fluctuation of the vibration amplitude, therefore, was likely due to the gusts in the wind. This is the same as stating that the unsteady response of the structure was likely due to buffeting. Also, the highly turbulent nature (the turbulence density was 12%) of the high-speed wind suggests that this vibration record could not have been induced by galloping, as galloping is primarily associated with the mean component of wind and turbulence destroys the necessary condition for galloping (Simiu and Scanlan 1996).

Figure 24 Displacement time history of a segment of steady vibration
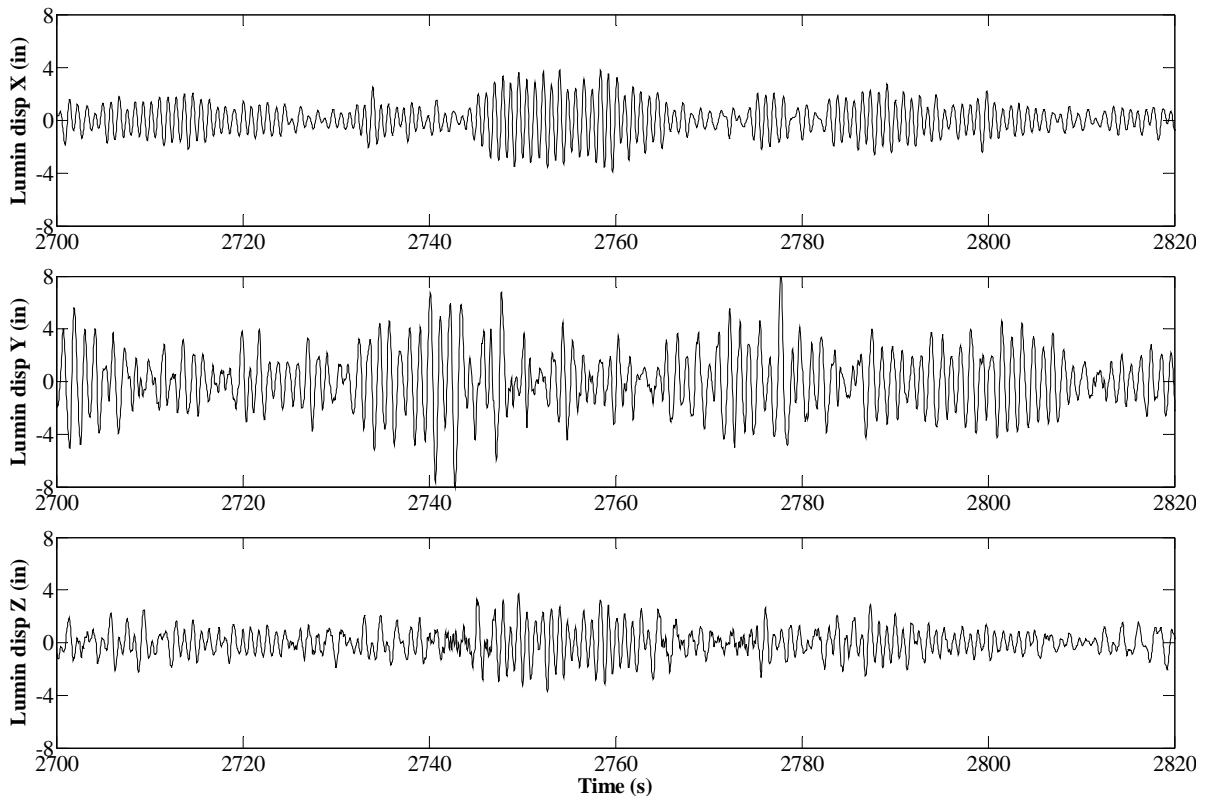
Figure 25 Displacement time history of a segment of unsteady vibration
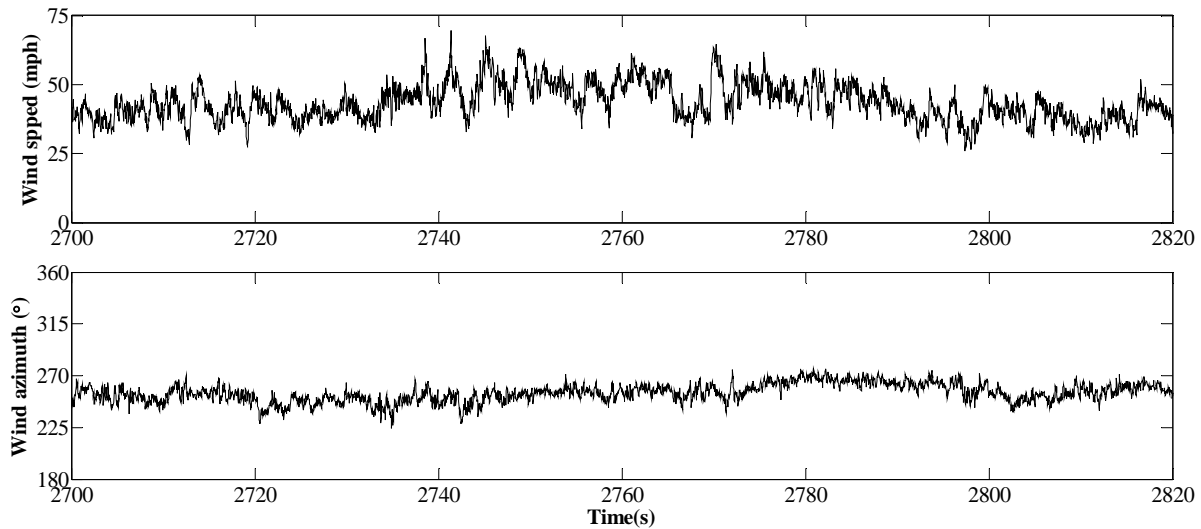
Figure 26 Wind speed and direction associated with the unsteady vibration shown in Figure 25

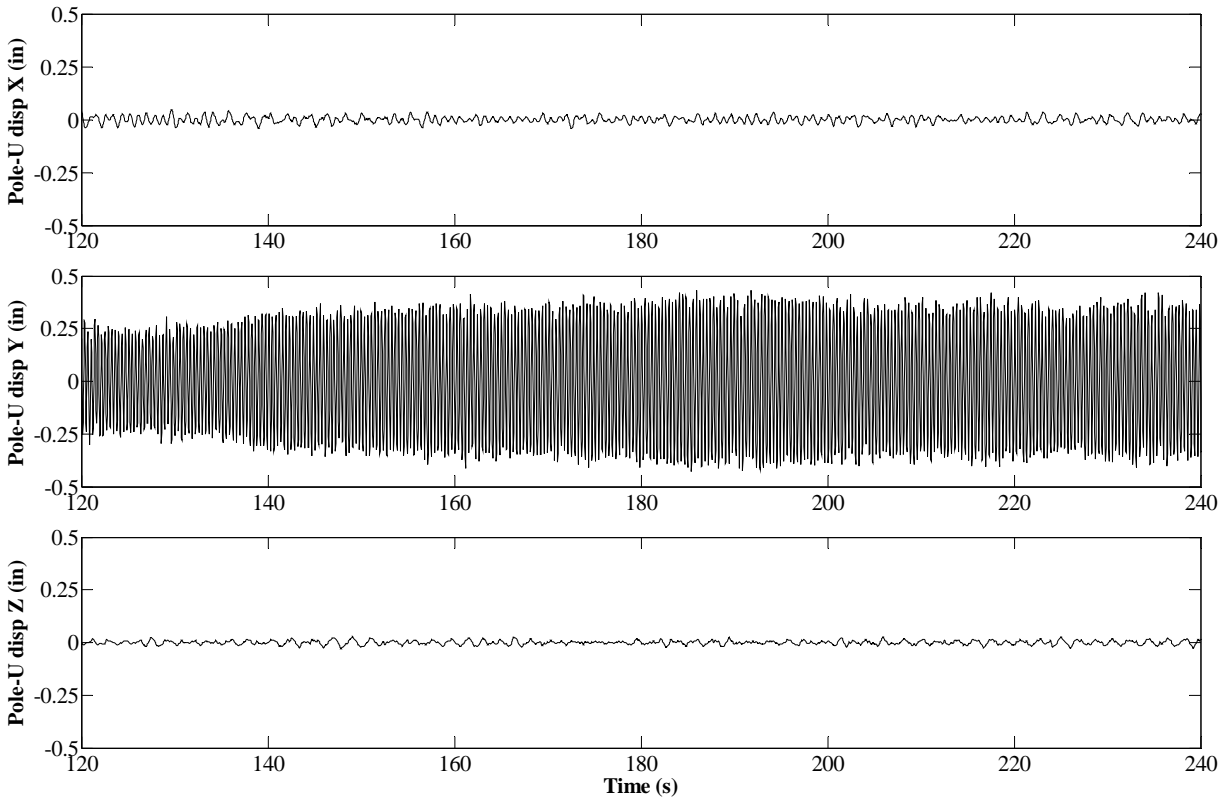The unsteadiness of the vibrations in category one and the steadiness of those in category two also manifested themselves in the maximum amplitude to RMS amplitude ratio of the 30-second segments. Figure 27 (a) and (b) shows this ratio for the vibrations in category one and category two, respectively. It is evident that the average ratio for vibrations in category one are much higher than that of the vibrations in category two. This is an indication that the vibration amplitudes in the category one exhibited much more fluctuation than did the vibrations in category two. Again, this highly unsteady nature of category one vibrations suggests that they were likely due to buffeting. On the other hand, the steadiness of category two vibrations further enhances the suggestion that they were induced by vortex-shedding.
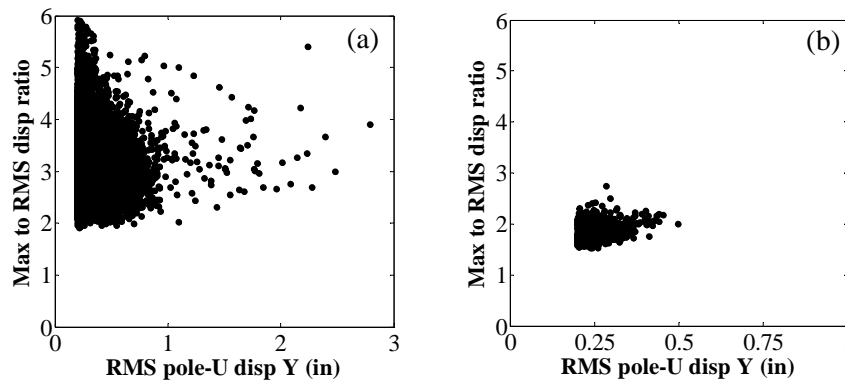
Figure 27 Maximum amplitude to RMS amplitude ratio for two categories of vibration

Figure 27 also suggests that the maximum amplitude to RMS amplitude ratios were significantly higher than $\sqrt{2}$, which is the ratio for signals that are sinusoidal. This is true even for the relatively steady vibrations in category two. This fact must be noted when the RMS amplitudes are used in the interpretation of the vibrations so that the severity of the vibrations are not underestimated. In addition, the highly unsteady nature of the vibrations in category two is a primarily cause for the broad spread of the data in the graphs associated with this category of vibrations

Table 3 summarizes the characteristics of the vibrations presented in this section. Based on these observations, it can be concluded that the lighting pole is susceptible to two types on excitations. One type is buffeting, which result in high displacement amplitudes, and the other is vortex-shedding, which result in amplitudes that are moderate. More quantitative characterization of the vibrations will be presented in the next section.

Table 3 Observed characteristics of lighting pole vibration

	Category One	Category Two
Dependence on wind speed	Occurred over a broad range of wind speed; amplitude increase with increasing wind speed.	Wind speed restricted.
Dependence on wind direction	Occurred over a broad range of wind directions.	Only occurred over specific ranges of wind directions.
Dimensionality	Simultaneous participation of both in-plane and out-of-plane components.	Predominantly in one plane
Steadiness	unsteady	steady

6.2   Interpretation of Modal Characteristics of Observed Vibrations

To study the vibrations at a modal level, as described in Chapter 4, the displacement time histories were decomposed in to components in the significant modes using a six order band-pass Butterworth filter. The Hilbert transform was then used to estimate the instantaneous amplitudes and frequencies of the modal vibrations. The average amplitudes and frequencies were computed for every 30-second segment of the vibrations and stored in a relational database for statistical analysis purposes. In this section, the modal characteristics of the vibrations are interpreted in the context of wind speed and direction.

Figure 28 (a) plots the 30-second mean modal out-of-plane (Y) displacement amplitudes of the upper pole tip against the corresponding wind speed. Only vibration data with mean amplitude greater than 0.2 in are included in the graph. The two distinct categories of vibrations shown in Figure 18 are again present. The first category of vibration, whose amplitude increased with increasing wind speed, was primarily in the first mode, although vibration in the second mode also occurred at high wind speeds. The fact that significant vibrations in the second mode occurred only when wind speed were high indicates that these vibrations were likely induced by turbulence in the wind, as high frequency (e.g. at the frequency of the second out-of-plane mode, which is 3.65 Hz.) turbulence components only become relevant to structural oscillation when wind speed is high. The vibrations in category two, which occurred over a restricted wind speed range of approximately 4 mph to 9 mph, were all in the second mode. The fact that the second mode of vibrations in the category two occurred over a lower wind speed than did the primarily first-mode vibrations in the first category suggests strongly that the two categories of vibration were due to different excitation mechanisms.

Figure 28 (b) presents the modal vibration amplitude again the corresponding reduced velocity associated with wind speed. The reduced velocity is refined as

$$v_r = \frac{U}{f \cdot D} \tag{4}$$

where U is wind speed; f is the frequency of the modal vibration and D is a representative dimension of the body subjected to wind excitation. Obviously, for vortex-induced vibration, the reduced velocity is the reciprocal of the Strouhal number. Since the dimension of the lighting pole varies with location, the diameter of the pole at the same height of the anemometer, which is approximately 8 inches, was chosen as the representative dimension D. The wind speed was chosen as that measured by the anemometer. These selections of the parameters were not necessarily the most appropriate, since the pole is located in the lowest part of the atmospheric boundary layer, where wind speed varies significantly with height, and the location at which the pole was engaged by wind excitation could not be readily identified. Nonetheless, Figure 28 (b) completely differentiates the two categories of vibrations with their distinct dependence on reduced velocity. In particular, it can be observed that the vibrations in category two were clearly reduced-velocity restricted and that the highest-amplitude vibrations in this category occurred at reduced velocities close to 5, which is the reciprocal of the Strouhal number for circular cylinders. It can be concluded definitively, therefore, that the vibrations in the second category were due to vortex shedding and that the shedding occurred around the pole. On the other hand, compared to the vibrations in category two, both modes of vibration in category one occurred over a broad range of much higher reduced velocity, and the amplitude of the vibration increased with increasing reduced velocity. This fact is more evidence that the vibrations in the category two were likely induced by buffeting.

Figure 28 Mean modal amplitudes vs. (a) wind speed and (b) reduced velocity for vibrations of the upper pole tip in the Y direction

Figure 29 shows the correlation between the out-of-plane modal vibrations at the upper pole tip and corresponding wind directions. It can be observed again that significant out-of-plane vibrations in category two occurred only when wind approached in the in-plane direction of wind, that is, close to 90° or 270°. In contrast, the significant out-of-plane vibrations in category one did not appear to be dependent on wind direction.
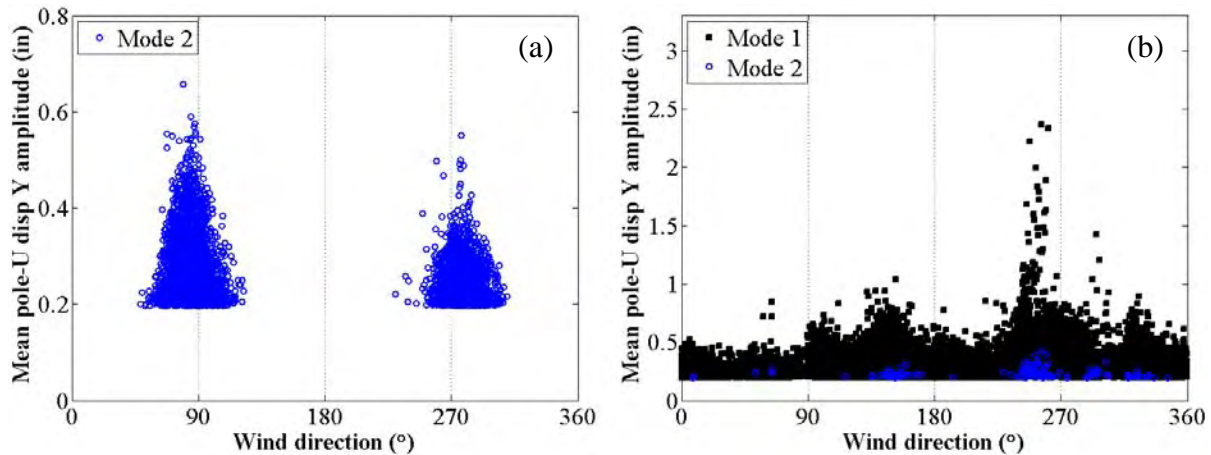
Figure 29 Correlation between modal displacements of the upper pole tip in the Y direction and wind direction for (a) category two and (b) category one

It appears in Figure 28 and Figure 29 that the vibrations of category one in the out-of-plane direction occurred mostly at quite low amplitudes. This is a false impression, however, due to the shape of this mode. Figure 30 illustrates the correlation between the modal out-of-plane (Y) displacement amplitudes of the luminaire and the corresponding wind speeds and reduced velocities. The two categories of vibration are again apparent in these graphs. For the same wind speed or reduced velocity, the amplitudes of the first out-of-plane mode at this location were apparently higher than those at the location of the upper pole tip. In contrast, the amplitudes of the second mode were at a lower level at the luminaire location than at the upper pole tip.
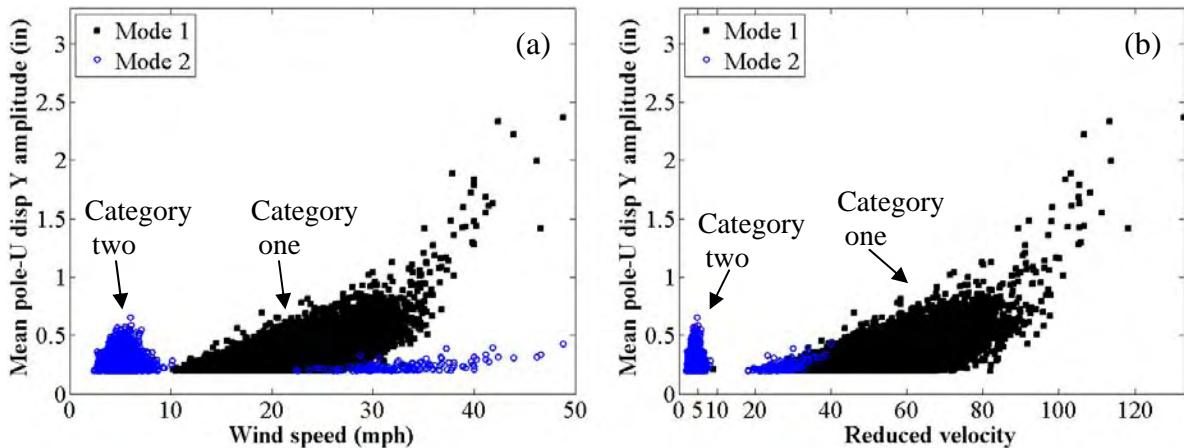

Figure 30 Mean modal amplitudes vs. (a) wind speed and (b) reduced velocity for vibrations of the luminaire in the Y direction

Figure 31 and Figure 32 show the correlation between the 30-second mean modal amplitudes of the vibrations in the Z direction and the wind speed, reduced velocity and wind direction. The Z component is chosen to represent the vibrations in the plane of the lighting pole because the vibration in the second mode in the X direction is limited by its mode shape at this location. Similar observations for the vibrations in the out-of-plane direction can be observed in these plots. Two differences should be noted in this case. The first is that the in-plane vortex-induced vibrations were due to wind approaching from close to the out-of-plane directions of the lighting

pole. (0° / 360° and 180°), which is perpendicular to the in-plane oscillations. The second is that the in-plane vortex-induced vibrations occurred over a slightly higher wind speed range than did the vortex-induced vibrations in the out-of-plane direction. This is because the frequency of the second in-plane mode (3.60 Hz) is higher than that of the second out-of-plane mode (2.70 Hz). The vortex-induced vibrations did occur over similar reduced velocity ranges according to Figure 28, Figure 30 and Figure 31.
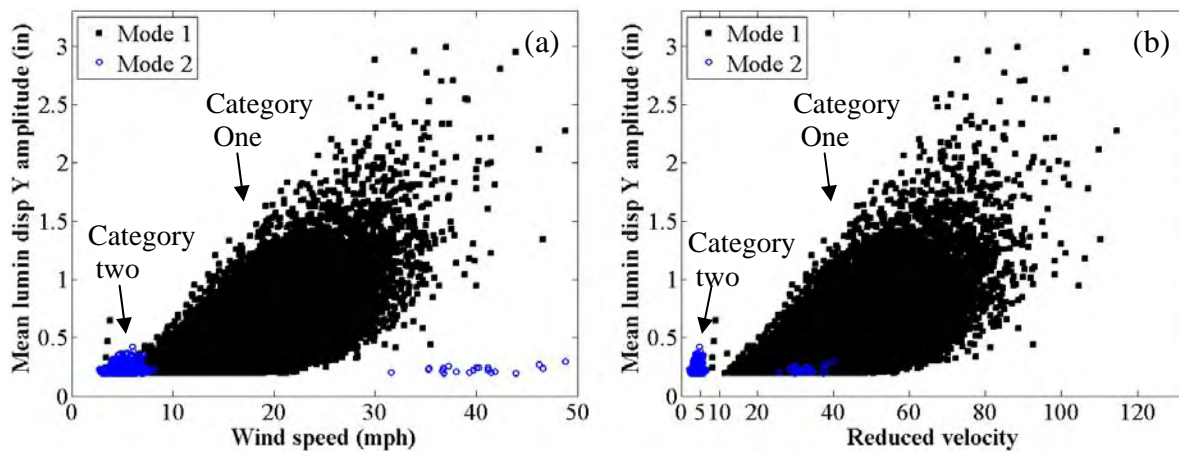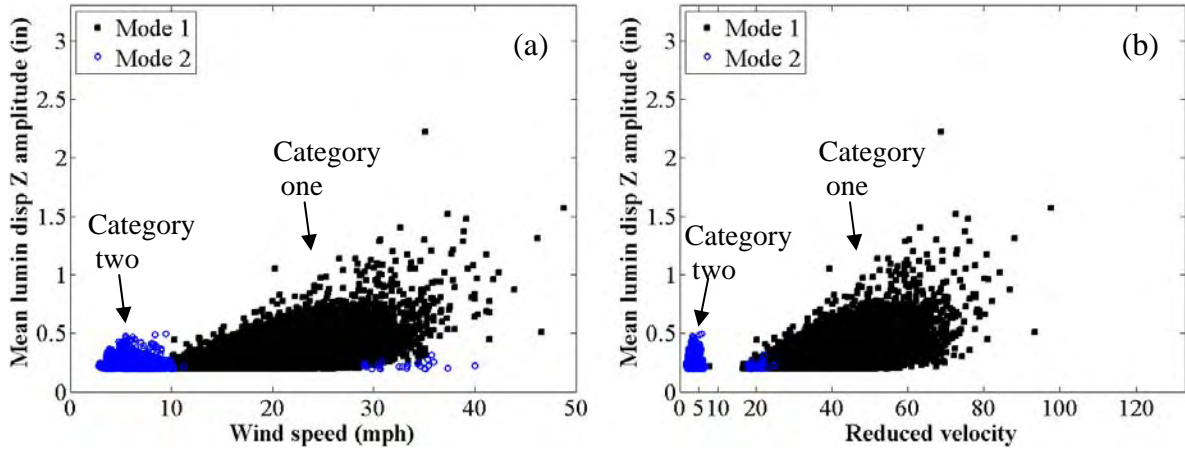

Figure 31 Mean modal amplitudes vs. (a) wind speed and (b) reduced velocity for vibrations of the luminaire in the Z direction
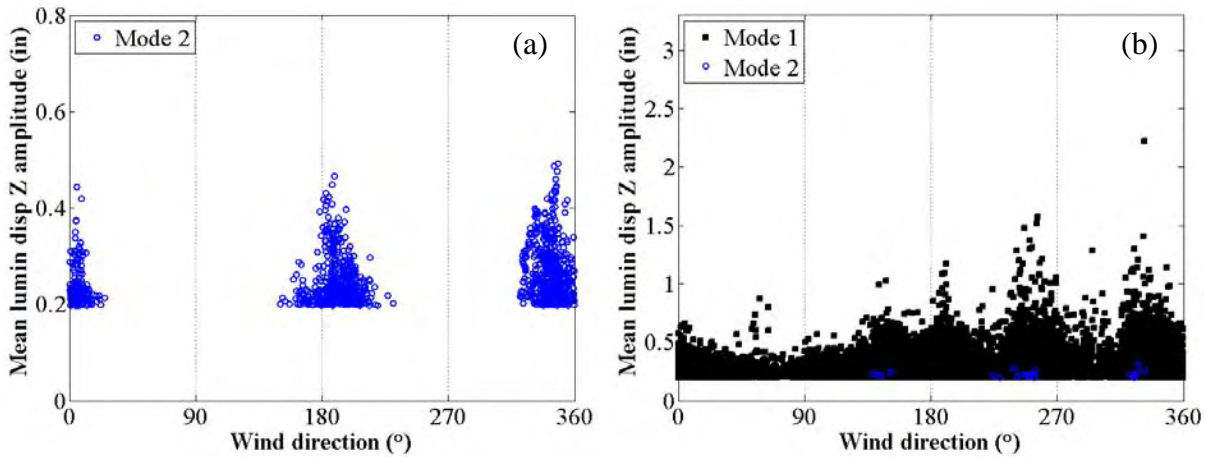
Figure 32 Correlation between modal displacements of the upper pole tip in the Y direction and wind direction for (a) category two and (b) category one

In addition to their different dependence on wind, the difference in the steadiness of the two categories of vibrations is also present in the modal components. For illustration purposes, Figure 33 and Figure 34 show two example modal vibration segments in the two categories, respectively. The component shown in Figure 33 is the second-mode out-of-plane vibration decomposed from the displacement segment shown in Figure 24; the component shown in Figure 34 is the first-mode out-of-plane vibration decomposed from the record shown in Figure 25. In addition to the apparent difference in the amplitude of the vibrations, it can be observed that the frequency of the modal component in category two was near-constant over the two minutes, while the frequency of the modal component in category two fluctuated significantly. The near-

constant nature of the instantaneous frequency is a characteristic of locked-in vortex-induced vibration, as vortex-shedding is inherently narrow-band. The fluctuation of the modal frequency is characteristic of buffeting-induced vibration as buffeting is broad-band in nature. It appears that in the latter case, the lighting pole was simply responding to the gusts of different frequency in the wind.
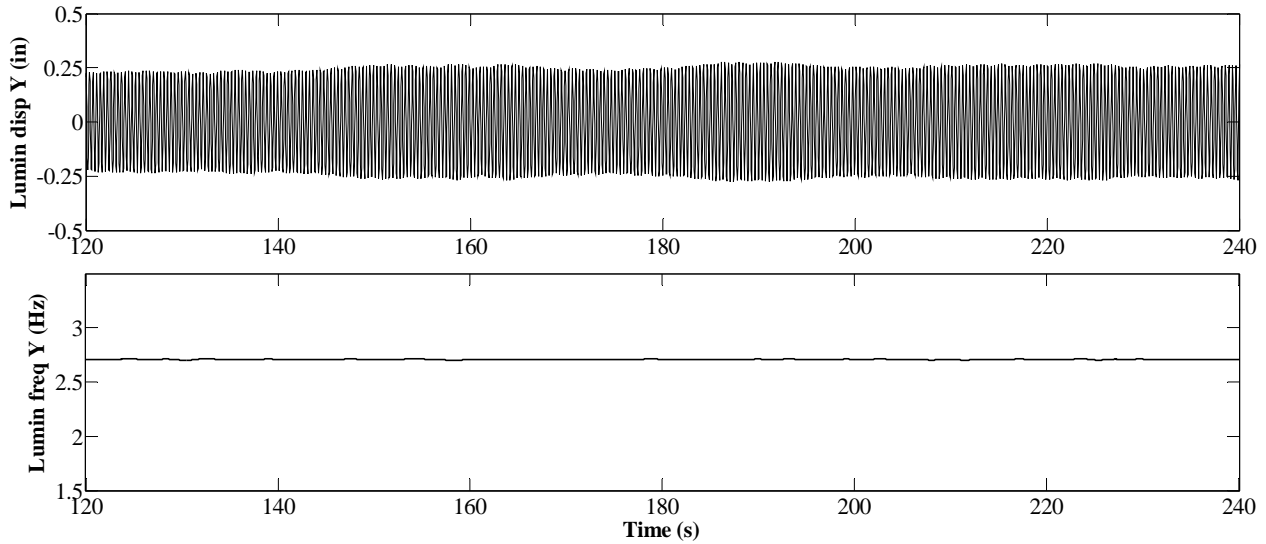
Figure 33 Time history and instantaneous frequency of a segemnt of a vibration component in category two

Figure 34 Time history and instantaneous frequency of a segment of a vibration component in category one

It has to be noted that although the term "modal component" has been used herein, such components really represent the vibration of the structure over a narrow frequency range that is centered at the natural frequencies of the individual modes, since the response of the lighting pole structure was amplified at frequencies close to its modal frequencies. The presence of the spikes in the instantaneous frequency of the unsteady vibration is due to the fact that the band-

pass filter did not completely filter out these components in the vibration. Nonetheless, the characteristics of the modal vibrations and their correlation with wind speed and direction presented in this section further validated the observation that the vibrations in category one were due to buffeting and that the vibrations in category two were due to vortex-shedding.

7 Conclusions and Recommendations for Future Study

This reported summarizes an effort to understand the wind-induced vibrations of a cantilever-armed highway lighting pole structure. The investigation was primarily based on full-scale monitoring of a 40 ft aluminum lighting pole erected at the Reese Technology Center of Texas Tech University.

The full-scale data were used in conjunction with numerical modeling to study the mode shapes and natural frequencies of the structure. It was revealed that the lower modes of the structure can be susceptible to wind excitation because the frequencies of these modes are low. A specific characteristic is that the in-plane and out-of-plane modes of the lighting pole are uncoupled due to the different structural configurations in these two planes. As observed, this to a large extent affected the response of the structure to wind. The damping characteristics of the structure in the fundamental modes in the in-plane and out-of-plane directions were evaluated using the logarithmic decrement method based on free decay data obtained from a series of manually forced vibration tests. The results suggest that the damping in the structure is vibration amplitude dependent, that it is at a low level and that it is different in the in-plane and out-of-plane directions.
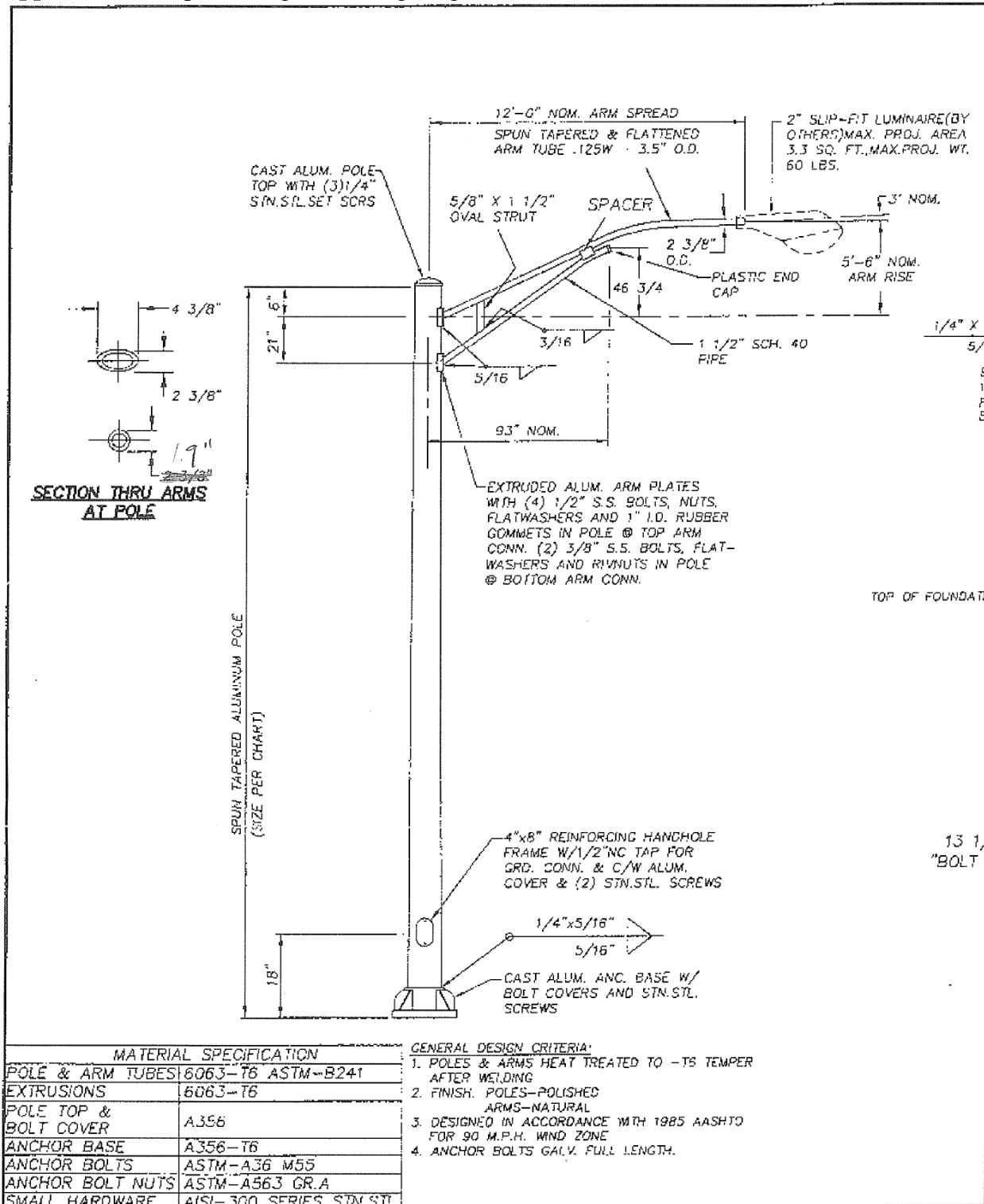
It was observed that the lighting pole exhibited two categories of vibrations under the excitation from wind. The first category occurred mostly in the first in-plane and out-of-plane modes of the structure at high wind speeds over a broad range of wind directions, and the amplitudes of the vibrations increased with increasing wind speed. The vibrations in this category are usually highly three-dimensional and are unsteady in nature. Since this category of vibration can reach quite high amplitude, they are potentially critical for the health of the structure. The second category of vibration occurred in the second in-plane and out-of-plane modes of the structure over a restricted range of low wind speed. In contrast to the first category of vibration, vibrations in this category were steady and restricted to one plane of the structure. They only occurred when wind approaches either from the in-plane or out-of-plane direction of the structure and the directions of the oscillations were always close to perpendicular to the mean direction of wind. These characteristics of the vibrations and their correlation with wind enable the identification of the first category of vibration to be buffeting induced and the vibrations in the second category to be vortex-induced. Since the buffeting-induced vibrations can reach quite high displacement amplitude, according to the full-scale data, they are potentially critical for the health of the structure. Although the displacement amplitudes of the vortex-induced vibrations were usually low, the stresses induced by these vibrations can be high since the oscillations were in the second in-plane and out-of-plane modes. Also, since the frequencies of vibration in these modes were high, this type of vibration goes through a larger number of cycles than the vibrations in the first modes do during the same period of time. Due to these reasons, vortex-induced vibrations should be included in the fatigue design of the lighting pole.

The understanding developed through this research effort can be used as a basis for future quantitative study of the wind loading on lighting pole structures. The fatigue behavior of the structure can be evaluated based on the incorporation of full-scale data and existing analytical models (e.g., Repetto and Solari 2001, Holmes 2002). In addition, the existing infrastructure and methodology utilized in this study can be used for future experimental studies, such as investigation of the behavior of other types of lighting pole (e.g. steel poles and glass-fiber composite poles, and poles with different types of luminaire) and the development and optimization of effective and economical mitigation devices for lighting pole vibrations. An example of the potential mitigation device is the chain impact damper. This simple form of the damping supplementing device has been used in existing lighting poles, but it is often used ad hoc. With the already developed understanding and the existing infrastructure, the performance of this device can be systematically studied with little investment.

References

AASHTO. (2001). *Standard specifications for structural supports for highway signs, luminaires and traffic signals (4th edition)*, American Association of State Highway and Transportation Officials, Washington DC, USA.

Bendat, J. S., and Piersol, A. G. (2000). *Random data analysis and measurement procedures (3rd edition)*, John Wiley and Sons, New York, NY, USA.

Caracoglia, L., and Jones, N. P. (2007). "Numerical and experimental study of vibration mitigation for highway light poles." *Engineering Structures*, 29(5), 821-831.

Clough, R., and Penzien, J. (2003). *Dynamics of structures*, 2nd Ed., Computers and Structures, Inc., Berkeley, California.

Connor, R. J., Hodgson, I. C., Callahan, G., Brakke, B., and Koob, M. (Year). "Field and Laboratory Studies on High-Mast Lighting Towers in Iowa." *2007 Mid-Continent Transportation Research Symposium, Iowa State University, Ames, IA*.

Den Hartog, J. P. (1956). *Mechanical Vibrations, 4th Edition*, McGraw-Hill, Inc. (now Dover Publications 1985), New York, NY.

Dexter, R. J. (2004). "Investigation of cracking of high-mast lighting towers." *Research Report*, Iowa Department of Transportation, Office of Bridges and Structures, Ames, IA, USA.

Dowell, E. H., and Crawley, E. F. (1995). *A modern course in aeroelasticity*, 3rd Ed., Kluwer Academic Publishers.

Foley, C. M., Ginal, S. J., Peronto, J. L., and Fournelle, R. A. (2004). "Structural analysis of sign bridge structures and luminaire supports." *Wisconsin DOT Report 04-03*, Department of Civil and Environmental Engineering, Marquette University, Milwaukee, Wisconsin, USA.

Fung, Y. C. (2002). *An Introduction to the Theory of Aeroelasticity*, Dover.

Holmes, J. D. (2002). "Fatigue life under along-wind loading - closed-form solutions." *Engineering Structures*, 24(1), 109-114.

Kaczinski, M. R., Dexter, R. J., and Van Dien, J. P. (1998). "Fatigue Resistance Design of Cantilevered Signal, Sign and Light Supports." *(NCHRP Report 412 - Project 10-38)*, ATLSS Engineering Research Center, Bethlehem, PA.

McDonald, J. R., Mehta, K. C., Oler, W., and Pulipaka, N. (1995). "Wind Load Effects on Signs, Luminaires and Traffic Signal Structures." *Texas Department of Transportation Report No. 1303-1F*, Wind Engineering Research Center - Texas Tech University, Lubbock, TX.

Mitra, S. K. (2004). *Digital Signal Processing: A Computer Based Approach*, McGraw-Hill Companies.

Peil, U., and Behrens, M. (2002). "Fatigue of tubular steel lighting columns under wind load." *Wind and Structures*, 5(5), 463–478.

Repetto, M. P., and Solari, G. (2001). "Dynamic alongwind fatigue of slender vertical structures." *Engineering Structures*, 23(12), 1622-1633.

Simiu, E., and Scanlan, R. H. (1996). *Wind effects on structures*, 3rd edition Ed., John Wiley and Sons, New York, NY, USA.

Van de Lindt, J. W., and Goode, J. S. (2006). "Development of a reliability-based design procedure for high-mast lighting structural supports in Colorado. Selection Guide AASHTO Detail Category E." *Supplemental to Report SRR-91*, Colorado Department of Transportation, Safety and Traffic Engineering Branch.

SECTION THRU ARMS AT POLE

12'-6" NOM. ARM SPREAD

SPUN TAPERED & FLATTENED ARM TUBE .125W · 3.5" O.D.

2" SLIP-FIT LUMINAIRE(BY OTHERS)MAX. PROJ. AREA 3.3 SQ. FT.,MAX.PROJ. WT. 60 LBS.

CAST ALUM. POLE TOP WITH (3)1/4" STN.STL.SET SCRS

5/8" X 1 1/2" OVAL STRUT

SPACER

3" NOM.

2 3/8" O.D.

PLASTIC END CAP

5'-6" NOM. ARM RISE

46 3/4

4 3/8"

2 3/8"

3/16

1 1/2" SCH. 40 PIPE

5/16

93" NOM.

EXTRUDED ALUM. ARM PLATES WITH (4) 1/2" S.S. BOLTS, NUTS, FLATWASHERS AND 1" I.D. RUBBER GOMMETS IN POLE @ TOP ARM CONN. (2) 3/8" S.S. BOLTS, FLAT-WASHERS AND RIVNUTS IN POLE @ BOTTOM ARM CONN.

SPUN TAPERED ALUMINUM POLE (SIZE PER CHART)

TOP OF FOUNDATI

4"x8" REINFORCING HANDHOLE FRAME W/1/2"NC TAP FOR GRD. CONN. & C/W ALUM. COVER & (2) STN.STL. SCREWS

13 1/
"BOLT

1/4"x5/16"

5/16"

18"

CAST ALUM. ANC. BASE W/ BOLT COVERS AND STN.STL. SCREWS

MATERIAL SPECIFICATION	
POLE & ARM TUBES	6063-T6 ASTM-B241
EXTRUSIONS	6063-T6
POLE TOP & BOLT COVER	A356
ANCHOR BASE	A356-T6
ANCHOR BOLTS	ASTM-A36 M55
ANCHOR BOLT NUTS	ASTM-A563 GR.A
SMALL HARDWARE	AISI-300 SERIES STN.STL.

GENERAL DESIGN CRITERIA:
1. POLES & ARMS HEAT TREATED TO -T5 TEMPER AFTER WELDING
2. FINISH. POLES-POLISHED ARMS-NATURAL
3. DESIGNED IN ACCORDANCE WITH 1985 AASHTO FOR 90 M.P.H. WIND ZONE
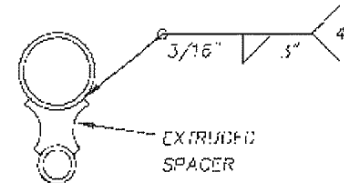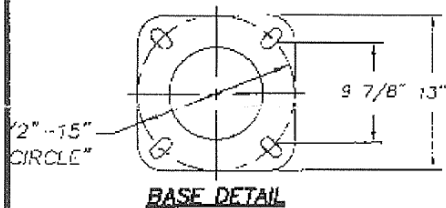4. ANCHOR BOLTS GALV. FULL LENGTH.

U.M. DESIGN NUMBER	U.M. MFG. HEIGHT	SPREAD	POLE TUBE SIZE
756-B108-Y1	40'-0"	12'-0"	.188-10.0"x6.0"x35'-0"

3121861R 1¼"x15"

B180-A224R0

FRAME TO HAVE 1/2-13
TAPPED HOLE IN LUG
(GROUNDING HARDWARE BY OTHERS)
1/4"-3/8" PROJ.

5/8" (REF)

1 1/2" (REF)

OVAL STRUT DETAIL

3/16"
6

ASE TAPPED
/4"-20
OR ATTACHING
OLT COVERS

5"

5 1/4"

1"

ON

(4) 1 1/4"x15" ANCHOR BOLTS W/
(4) HEX NUT, (3) FLAT WASHER,
& (1) LW EACH, FULL GALV

3/16"   5"   4
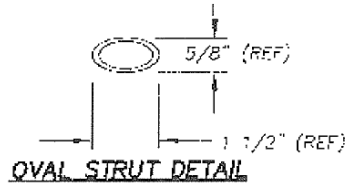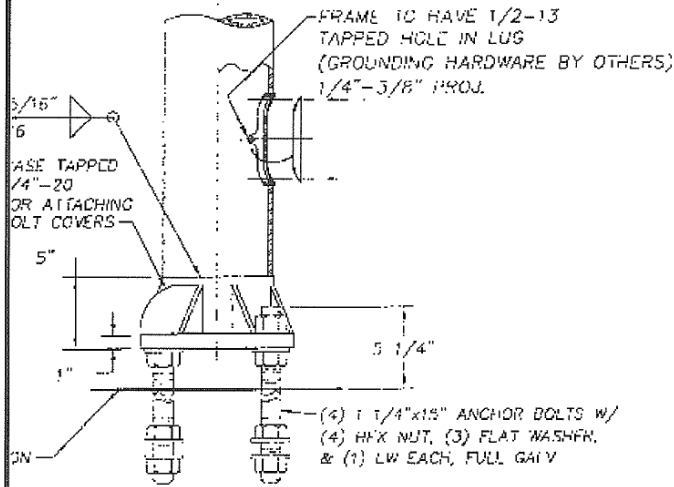
EXTRUDED
SPACER

EXTRUDED SPACER DETAIL

HANDHOLE DETAIL "A"-"A"

9 7/8" 13"

'2"-15"
CIRCLE"

BASE DETAIL

STATE OF TEXAS
JOHN MICHAEL FRITZ
92371
LICENSED
PROFESSIONAL ENGINEER

5/27/04

ALUMINUM LIGHTING POLES
NUECES COUNTY, TX
JFK BRIDGE, PROJ. NO. HP317(1)

LOF	ENG.REF.# 756-C81
REQ.# DTX44420-1 S.O.#	CAD#

Union Metal
CORPORATION

DRAWN PVC	DRAWING NO.
DATE 5/19/04	756-B108
CHECKED OKC	

REVISIONS

ORIGINAL